Hera-B 97–085
Target 97–004

7th May 1997

Wire Target Geometry and Tagging Performance

Thomas Lohse

Humboldt University, Berlin

Contents

1 Introduction

The tagging signatures for the flavour of B mesons produced at HERA-B are complicated by the high interaction rates which imply several superimposed interactions per bunch crossing. The design of the target wire configuration has to be optimized such that the interference between independent interaction vertices is as small as possible, i.e. the distance between the $b\bar{b}$ interaction vertex (in the following called B vertex) and other interaction vertices (in the following called minimum bias (MB) vertices) has to be maximized.

In this note the tagging procedures described in the HERA-B proposal are revisited for a systematic investigation of the sensitivity of the tagging powers to the width of the beam halo and a systematic study of various wire geometry layouts.

It is instructive to start with a simple analytical estimate of the overlap probability of the B vertex with any of the MB vertices. If one assumes that the target consists of N_W wires which are spatially well separated from each other and therefore independent, and if the number of MB interactions per bunch crossing follows a poisson distribution with mean value $\bar{N}_{MB}$, then the average number of MB interactions occuring on the same wire with the B vertex is $\bar{N}_{MB}/N_W$. If σ_{Halo} is the width of the gaussian halo at the wire and d_{min} is a critical distance, below which a MB vertex cannot any longer be separated from the B vertex, then the number of MB vertices which are merged with the B vertex at position x along the wire is distributed according to a poisson distribution with mean value

$$\bar{N}_{merge}(x) \;=\; \frac{\bar{N}_{MB}}{N_W} \cdot \int_{(x-d_{min})/\sigma_{Halo}}^{(x+d_{min})/\sigma_{Halo}} g(t)\,\mathrm{d}t \quad ,$$

where

$$g(t) \;=\; \frac{1}{\sqrt{2\pi}} \exp\left(-\frac{t^2}{2}\right)$$

is the normal distribution function. The probability $P(d_{min})$ that any of the MB vertices merges with the B vertex is hence

$$P(d_{min}) \;=\; 1 \;-\; \int_{-\infty}^{+\infty} \mathrm{d}u\, g(u) \cdot \exp\left[-\frac{\bar{N}_{MB}}{N_W} \cdot \int_{u-\frac{d_{min}}{\sigma_{Halo}}}^{u+\frac{d_{min}}{\sigma_{Halo}}} g(t)\,\mathrm{d}t\right] \quad . \tag{1}$$

This probability is displayed in Fig. 1 as a function of the halo width for five different values of d_{min} and for targets consisting of a single wire, four wires, or eight wires. The average number of MB vertices accompanying the B vertex is assumed to be $\bar{N}_{MB} = 4$. As will be shown below, the critical distance for tagging purposes concerning the CP violation measurement in the golden decay $B^0 \to J/\psi K_S^0$ is roughly $d_{min} \approx 200\,\mu$m. At this distance, and for a realistic halo width of $\sigma_{Halo} \approx 500\,\mu$m, one finds that the merging probabilities are ≈55% for a single-wire target, ≈20% for a four-wire target, and ≈10% for an eight-wire target (the latter presently installed in the experiment).

Although these numbers are instructive, it is very hard to predict, how sensitively the tagging power will react to them. In this note the complete tagging procedure, as developed in the proposal, is hence confronted quantitatively with a large variety of beam parameters and target configurations.

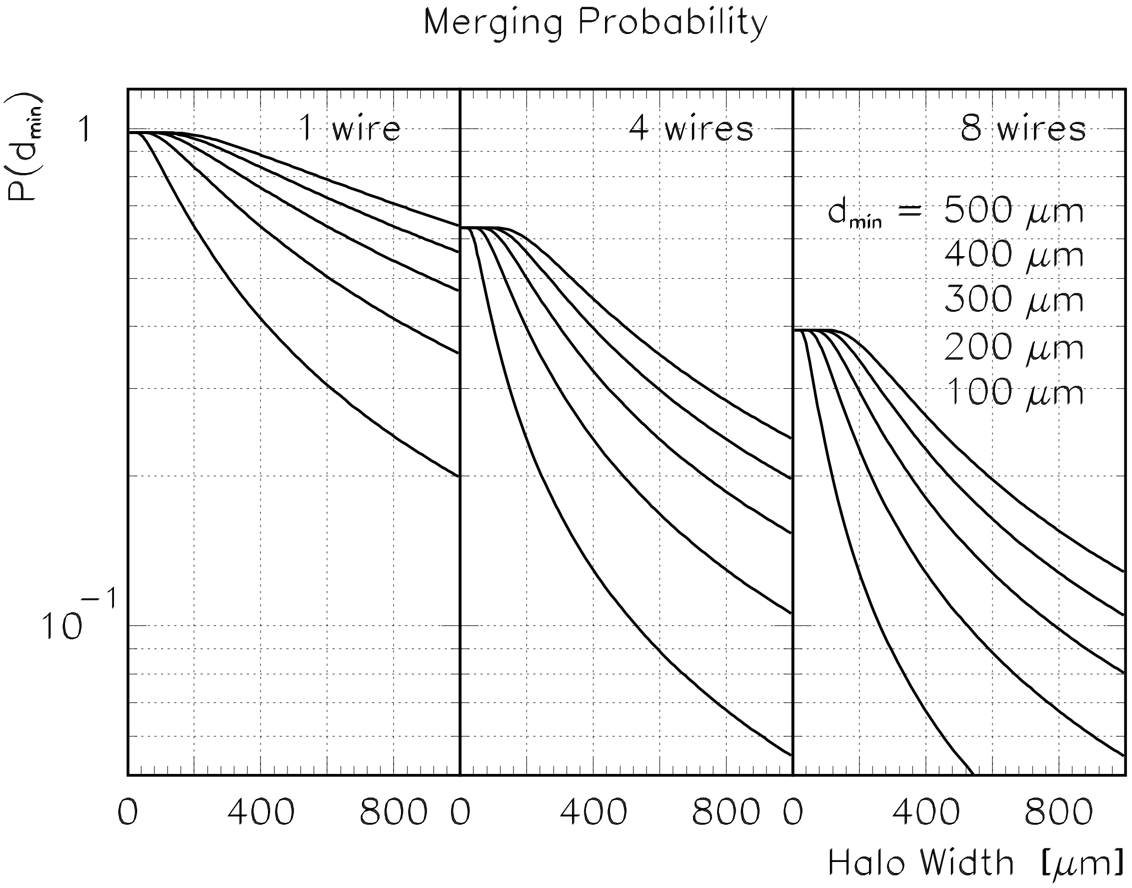

Figure 1: *Probability for merging of the B vertex with any MB vertex as a function of the r.m.s. halo width. The five curves correspond to five different assumptions for the critical distance d_{min}, below which a MB vertex cannot any longer be separated from the B vertex. The average number of MB vertices accompanying the B vertex is assumed to be $\bar{N}_{MB} = 4$ throughout. The three pictures correspond to targets consisting of a single wire (left), four wires (middle) and eight wires (right).*

The study is performed with a sample of Monte Carlo events (generated by the PYTHIA and FRITIOF generators as implemented in ARTE) where a golden B decay $B^0 \to J/\psi K_S^0$ is superimposed with an average of 4 MB events. The B decay simulation was modified in order to correctly include all effects of flavour mixing.

The wires are assumed to consist of aluminum of rectangular cross section ($\sqrt{12} \cdot 30\,\mu$m perpendicular to the beam direction, times $\sqrt{12} \cdot 100\,\mu$m along the beam direction). They are arranged either in two groups of wires in a distance of 5 cm along the beam, in close correspondence to the actual target, or in a single group at the longitudinal position closer to the vertex detector. Since the sensitivities to variations in the wire geometry turned out to be very mild, no attempt was made to achieve an even more detailed correspondence to the actual HERA-B target.

Contrary to the actual target design also situations in which the two target wire groups are azimuthally rotated relative to each other by an angle φ_{Group} are considered since this might improve the overall vertex separation.

Table 1 lists the combinations of target configurations and beam parameters which have been simulated. For each situation the simulated interactions were randomly distributed according to wire geometry and halo width. All tracks were run through a fast tracking simulation which uses the actual geometry of the vertex detector, combined with an older version of the main tracker (status of the TDR). Multiple scattering is taken into account but bremsstrahlung, decays in flight and secondary interactions are ignored completely.

Ideal pattern recognition is assumed, i.e. a track can only be lost if it is outside the geometrical acceptance. Ghost tracks do not occur in this procedure. After the track reconstruction, the $B^0 \to J/\psi K_S^0$ decay is reconstructed by the HERA-B vertex package including all mass constraints. Primary vertices are then searched for by the vertex pattern recognition program in the vertex package (using untuned default steering parameters). The B vertex is always reconstructed: Either the B^0 reconstructed from the golden decay is assigned to a primary vertex by the pattern recognition, or a B vertex is computed from the intersect of the B^0 direction of flight with the closest wire of the target. After primary vertices are found and tracks assigned, the secondary vertex pattern recognition (with default steering parameters) is run in order to prepare the study of charge tagging.

2 Systematic Study of Primary Vertex Recognition

Before applying the full apparatus for B tagging, it is interesting to study the capabilities of the HERA-B detector to disentangle the B vertex from a closeby MB vertex.

In the HERA-B proposal it has been shown that two MB vertices start to affect each other (merged vertices, distorted vertices or ghost vertices appear) when they come closer than $400\,\mu$m. This number is not necessarily relevant for B/MB vertex separation. This is demonstrated in Fig. 2, where the distribution of standard deviations of the reconstructed vertex positions along the wire direction are displayed for B vertices and MB vertices. The quality of the B vertex is significantly superior to that of the MB vertex, a consequence of the high quality of the reconstructed B^0 "track" on the B vertex.

In order to cleanly investigate the limitations in vertex separation, one B vertex and one MB vertex were generated on a single target wire for a wide range of distances d of the two

Configuration	#groups	#wires per group	φ_{Group}	σ_{Halo} [mm]
1	1	1	–	0.10
2	1	1	–	0.25
3	1	1	–	0.50
4	1	1	–	1.00
5	1	1	–	2.00
6	1	4	–	0.10
7	1	4	–	0.25
8	1	4	–	0.50
9	1	4	–	1.00
10	1	4	–	2.00
11	2	4	0°	0.10
12	2	4	0°	0.25
13	2	4	0°	0.50
14	2	4	0°	1.00
15	2	4	0°	2.00
16	2	4	45°	0.10
17	2	4	45°	0.25
18	2	4	45°	0.50
19	2	4	45°	1.00
20	2	4	45°	2.00
21	2	8	0°	0.10
22	2	8	0°	0.25
23	2	8	0°	0.50
24	2	8	0°	1.00
25	2	8	0°	2.00
26	2	8	22.5°	0.10
27	2	8	22.5°	0.25
28	2	8	22.5°	0.50
29	2	8	22.5°	1.00
30	2	8	22.5°	2.00

Table 1: *Combination of target wire configurations and beam parameters considered for the systematic study of tagging performance.*

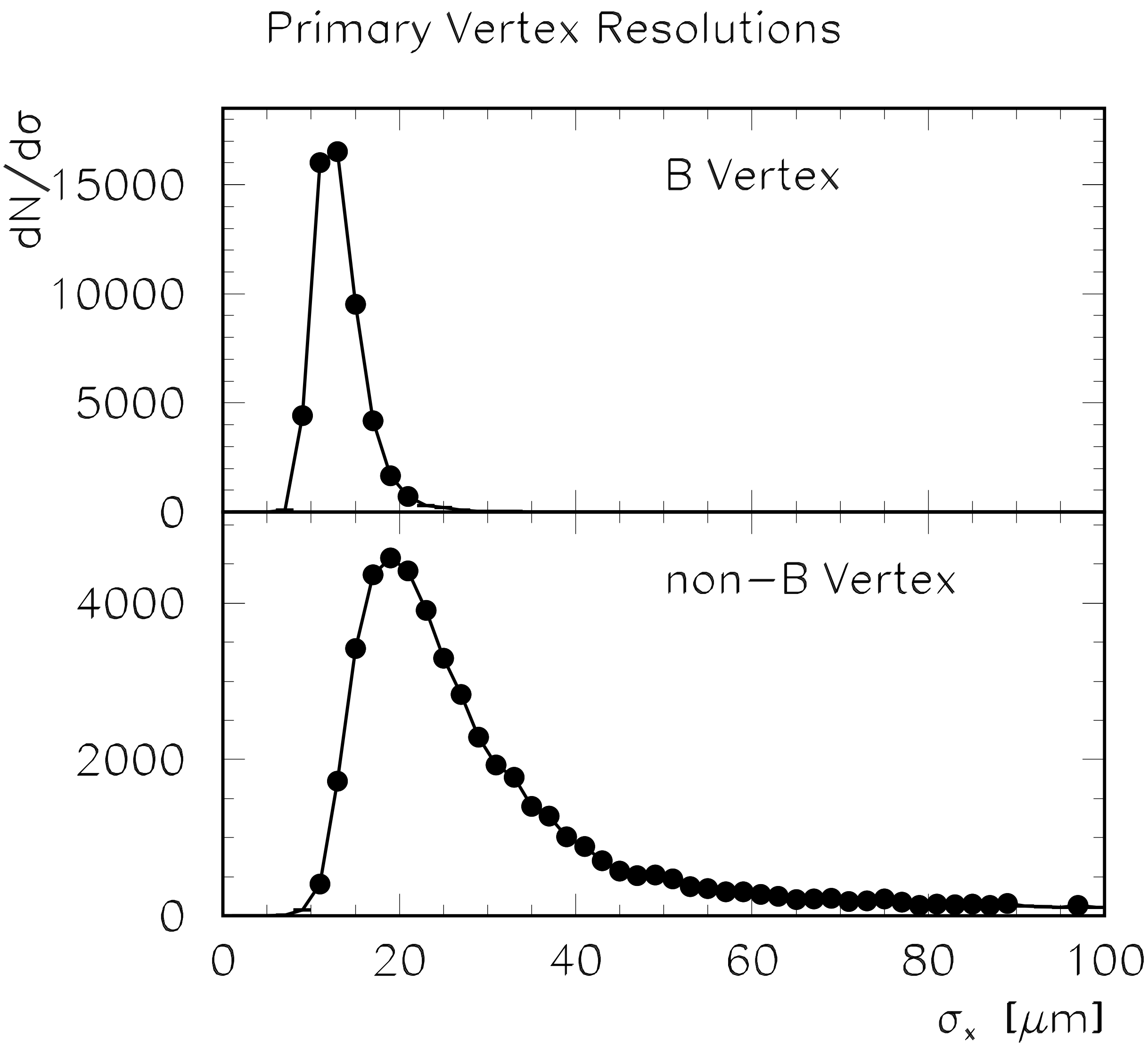

Figure 2: *Distribution of standard deviations for the vertex position along the target wire as obtained from the vertex fits for B vertices (upper plot) and MB vertices (lower plot).*

vertices along the wire direction. These simulated events were then passed through the full reconstruction chain as described in the introduction.

Fig. 3 displays the probabilities for finding only the B vertex (MB vertex is lost), for finding two vertices (both vertices found or MB vertex lost but fake MB vertex found) and for finding more than two vertices (at least one fake vertex found) as a function of d. As can be seen, the probability that the MB vertex is lost is larger than 10%, a trivial result of the cut on the minimum track multiplicity of a MB vertex. Also the probability of a fake MB vertex is larger than 10%. It is mostly due to splitting of the B vertex since the B vertex is composed out of tracks originating on the wire and tracks from secondary decays which miss the wire and the primary vertex by finite impact parameters. When $|d|$ becomes smaller than 200...300 μm, the two generated vertices are merged with large probability. The probability for a single reconstructed vertex increases up to 80%, the efficiency for finding an additional MB vertex drops down to 20% and the probability for ghost vertices basically vanishes.

When the two vertices start to merge, their positions are slightly distorted. This effect can be seen in Fig. 4 which shows the mean residual of the vertex position along the wire direction with respect to the generated position as function of d for the B vertex and the MB vertex. The vertices affect each other for distances less than 200 μm, but the distortions are very small as compared to typical impact parameter resolutions of tracks.

The tagging quality can be affected, once tracks from the B vertex are assigned to the MB vertex (loss of efficiency) or tracks from the MB vertex are assigned to the B vertex (additional dilution of the CP signal). If one assignes, for the sake of simplicity, each track to the closest vertex in space, no matter how big the distance is, (instead of more involved χ^2 distance procedures), one finds the track assignment probabilities as displayed in Fig. 5 as functions of d. The following effects are apparent:

- Assignment of tracks from the tagging B decay to the B vertex: The probability for this assignment is significantly smaller than 1 even for large d, which is a result of the fact that the B vertex can be split. This effect may reduce the tagging efficiency. When the MB vertex approaches the B vertex, the assignment probability first slowly decreases and then, at distances less than 200 μm when the vertices merge, sharply increases again to a maximum value since the MB vertex is not any longer reconstructable.

- Assignment of tracks from the tagging B decay to the MB vertex or a fake vertex: This probability is the complement of the preceding case. It is significant even for large d due to vertex splitting and is smallest for $d \approx 0$, when the vertices are merged and the vertex splitting is rare.

- Assignment of tracks from the MB vertex: When the two generated vertices are closer than 200 μm, the MB vertex is rarely reconstructed since it merges with the B vertex. Therefore all the MB tracks are in this case trivially assigned to the B vertex.

From all these observations it becomes apparent that severe effects from vertex merging can be expected when the distance of the B vertex and a MB vertex is smaller than 200 μm. In order to verify this, the efficiency of two of the most important cleaning cuts which are necessary for all tagging methods considered in this note were studied as function of d:

1. A tagging track must be closer than 1 mm (in three dimensional space) to the B vertex.

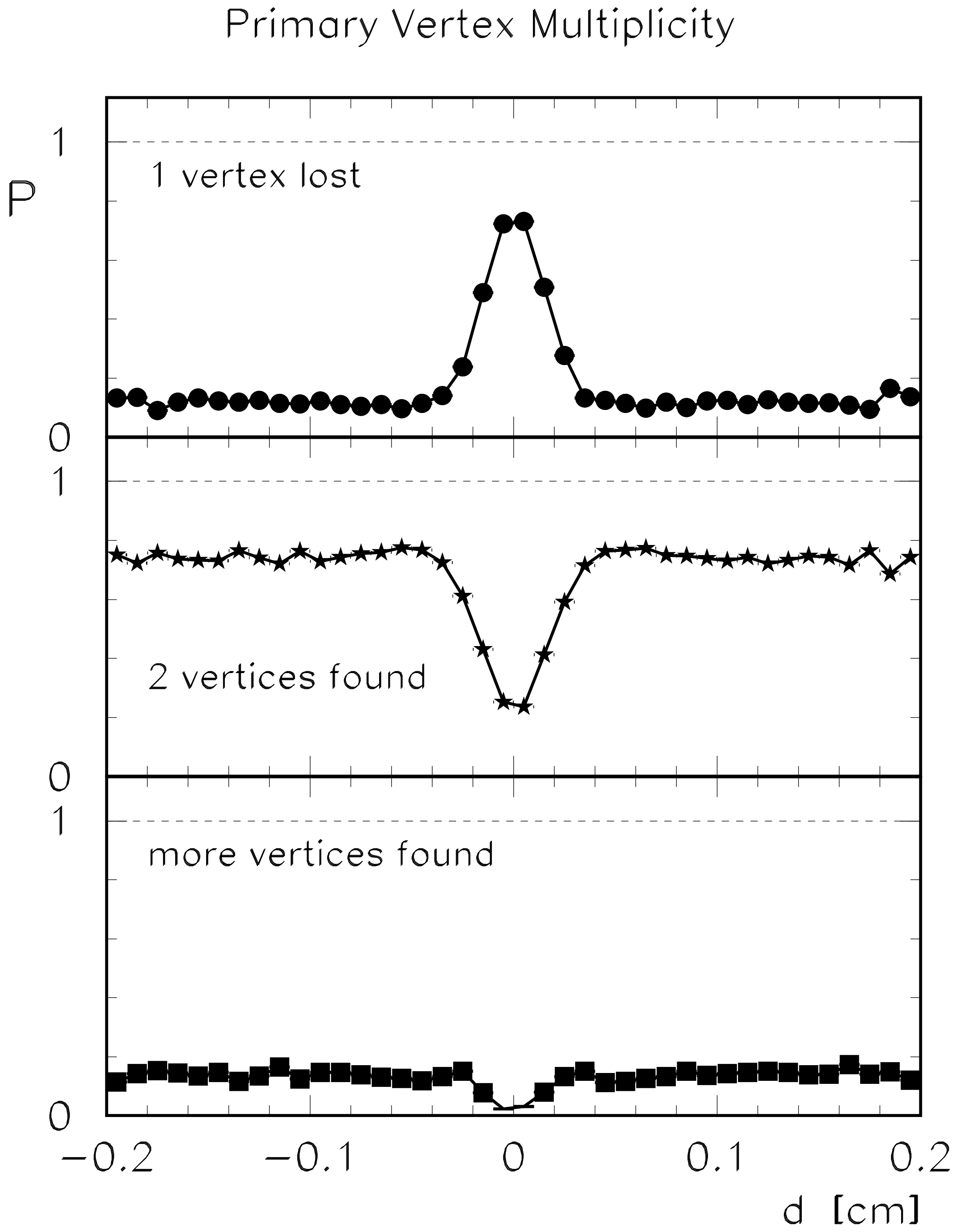

Figure 3: *Probabilities to reconstruct one, two, or more than two vertices as a function of the distance d along the wire direction between the generated B vertex and the generated MB vertex.*

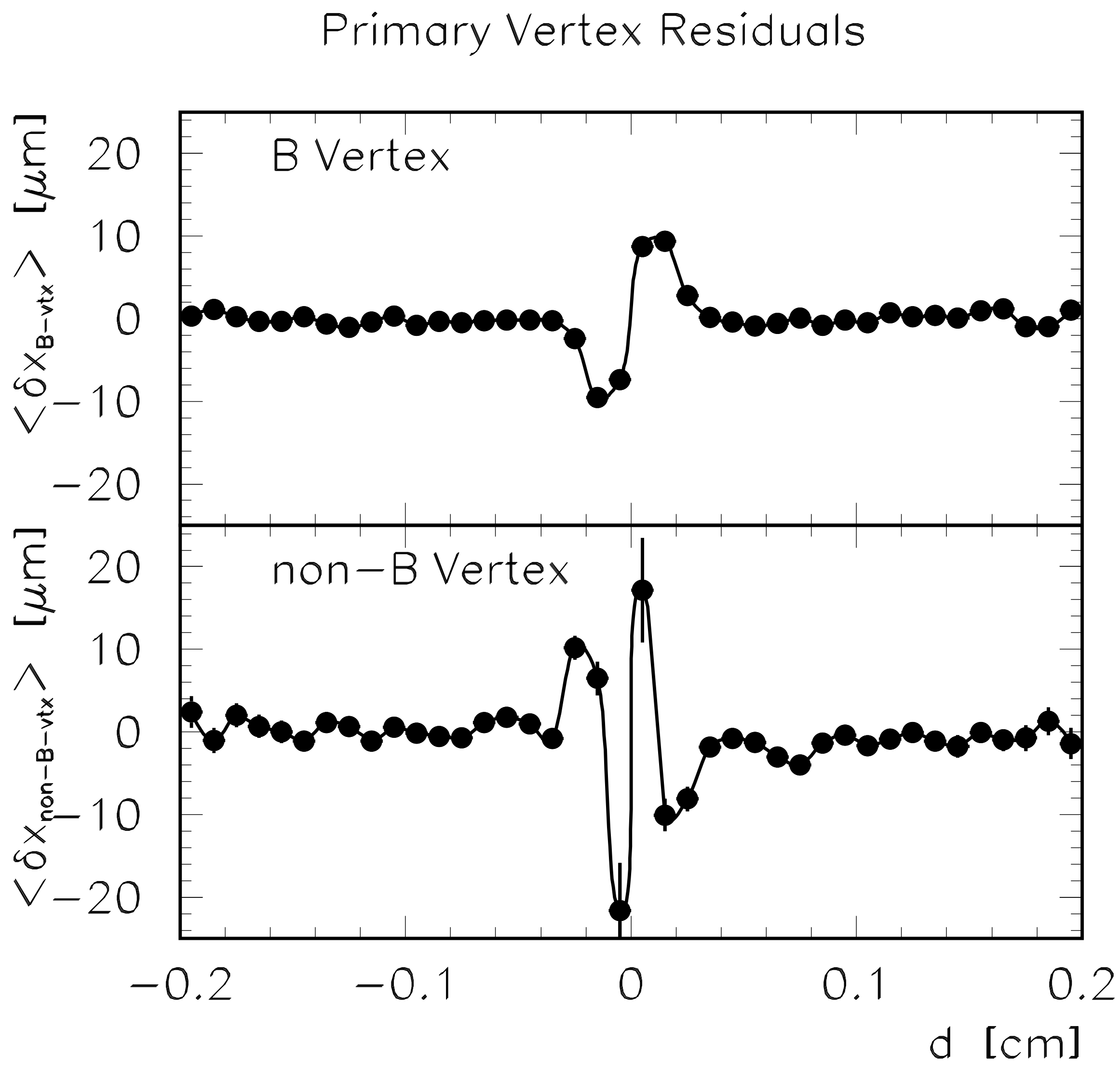

Figure 4: *Mean residuals of the reconstructed vertex positions along the wire direction with respect to the generated positions as function of the distance d between the B vertex and the MB vertex. The B vertex and the second reconstructed vertex are displayed separately.*

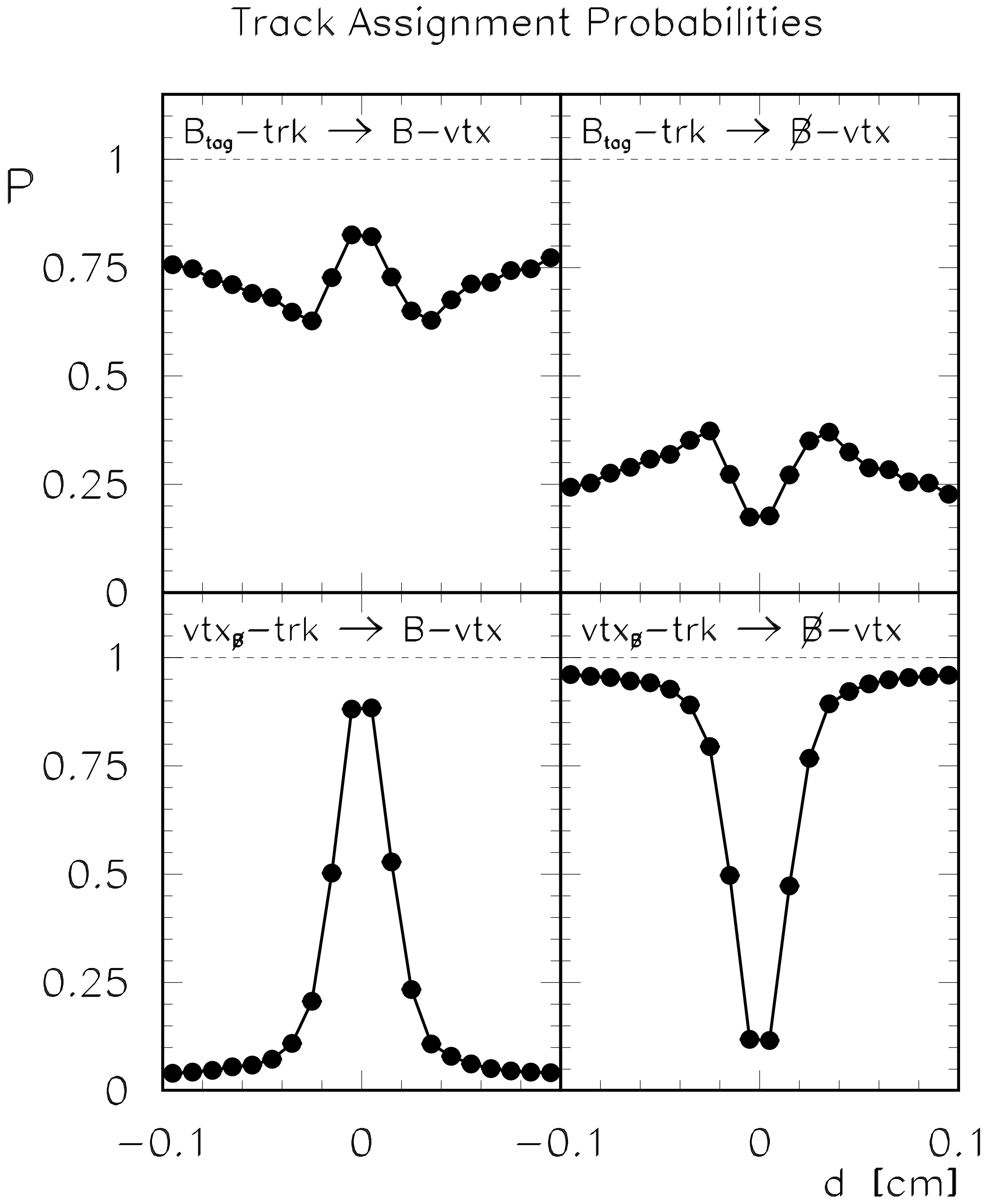

Figure 5: *Probabilities to assign a track from the decay of the tagging B particle to the B vertex or another reconstructed vertex (upper plots), and probabilities to assign a track from the MB vertex to the B vertex or another reconstructed vertex (lower plots) as function of the distance d between the generated B vertex and MB vertex.*

2. A tagging track must have a χ^2 distance larger than 4 from any reconstructed vertex apart from the B vertex itself.

In addition, all tags either use momentum cuts or momentum weighted quantities. Therefore only tracks with momentum larger than 5 GeV/c are considered here.

Firstly, in Fig. 6 the fraction of tracks from the decay of the tagging B particle surviving these cuts is shown. Since the distortion of the B vertex due to a closeby MB vertex is very small, it is not surprising that the tagging efficiencies stay almost completely unaffected by the vertex merging at small distances of the generated B vertex and MB vertex. Secondly, Fig. 7 shows the same cut efficiencies for tracks from reconstructed MB vertices (which are partially fake vertices split off from the B vertex). The cuts are very effective against these tracks which would dilute a CP violation signal, down to distances of $200\,\mu$m between the two generated vertices. At smaller distances the tracks from the MB vertex pass the cuts with high probability and hence represent a potential background for the tagging tracks. In order to judge the severeness of this background, all other requirements for a tagging track (especially those connected to particle identification or transverse momentum cuts) have to be considered quantitatively. In the next section, the tagging procedure will therefore be tested without artificially reducing the complexity of the problem.

3 Systematic Study of Wire Geometries

3.1 Primary Vertex Pattern Recognition

The quality of primary vertex pattern recognition has been tested for all the scenarios listed in table 1. In Fig. 8 the mean number of reconstructed primary vertices, $\langle n_{rec} \rangle$, normalized to the number of generated primary vertices, n_{gen}, is plotted as function of n_{gen} for all six wire configurations and three different values for the width of the beam halo. Note that the number of reconstructed vertices is always bigger than zero, since the B vertex is forced to be reconstructed. This explains why, on the average, n_{rec} is systematically larger than n_{gen} for small n_{gen}. When n_{gen} increases, the efficiency of primary vertex finding decreases strongly for the case of a single wire or a single group of 4 wires, while it stays quite stable and large up to highest vertex multiplicities for targets with more wires, as long as the halo width is at least $500\,\mu$m. The loss of vertices is of course especially severe in the case of a single wire, while in the case of a single group of four wires the vertex finding efficiency for $n_{gen} = 10$ is still bigger than 75% for $\sigma_{Halo} = 500\,\mu$m.

Of course, not all the primary vertices have to be necessarily reconstructed in order to perform the CP violation measurements. In fact, as can be concluded from section 2, the mild losses in the case of a four-wire target are dominated by merging of MB primary vertices, and not by the merging of the B vertex with a MB vertex. Therefore, a four-wire target might be fully adequate for the B physics goals of the experiment. The drastic losses of primary vertices for a single-wire target, on the other hand, look less encouraging and suggest some deterioration of the physics performance.

In the following subsections the different tagging methods are confronted in their detailed performance (cut by cut) with the the same wire configurations as studied in Fig. 8. The cuts are those applied in the proposal. No tuning has been attempted.

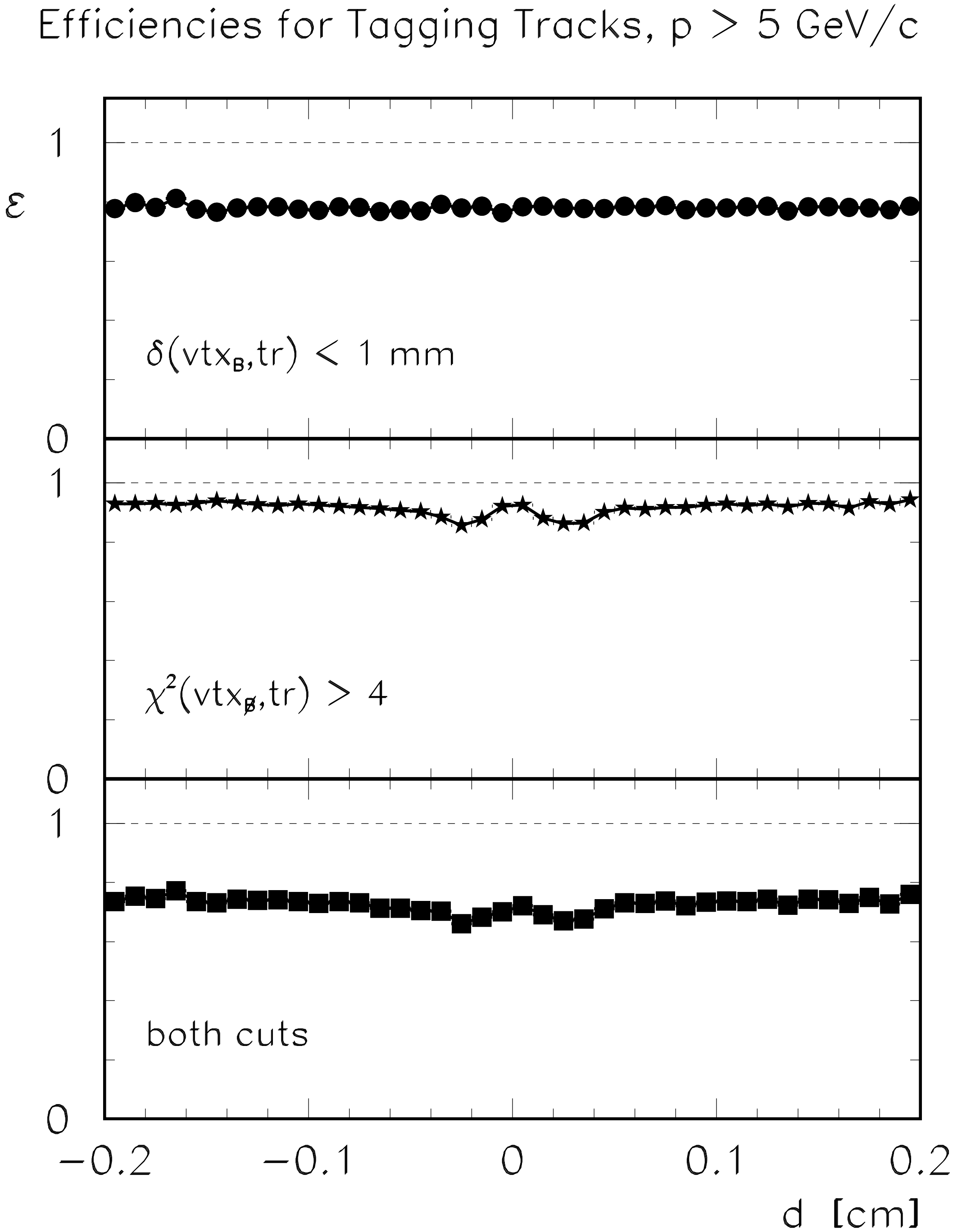

Figure 6: *Probabilities (as function of the distance d between the generated B vertex and MB vertex) for hard tracks from the tagging B decay to survive typical cleaning cuts applied in the tagging algorithms.*

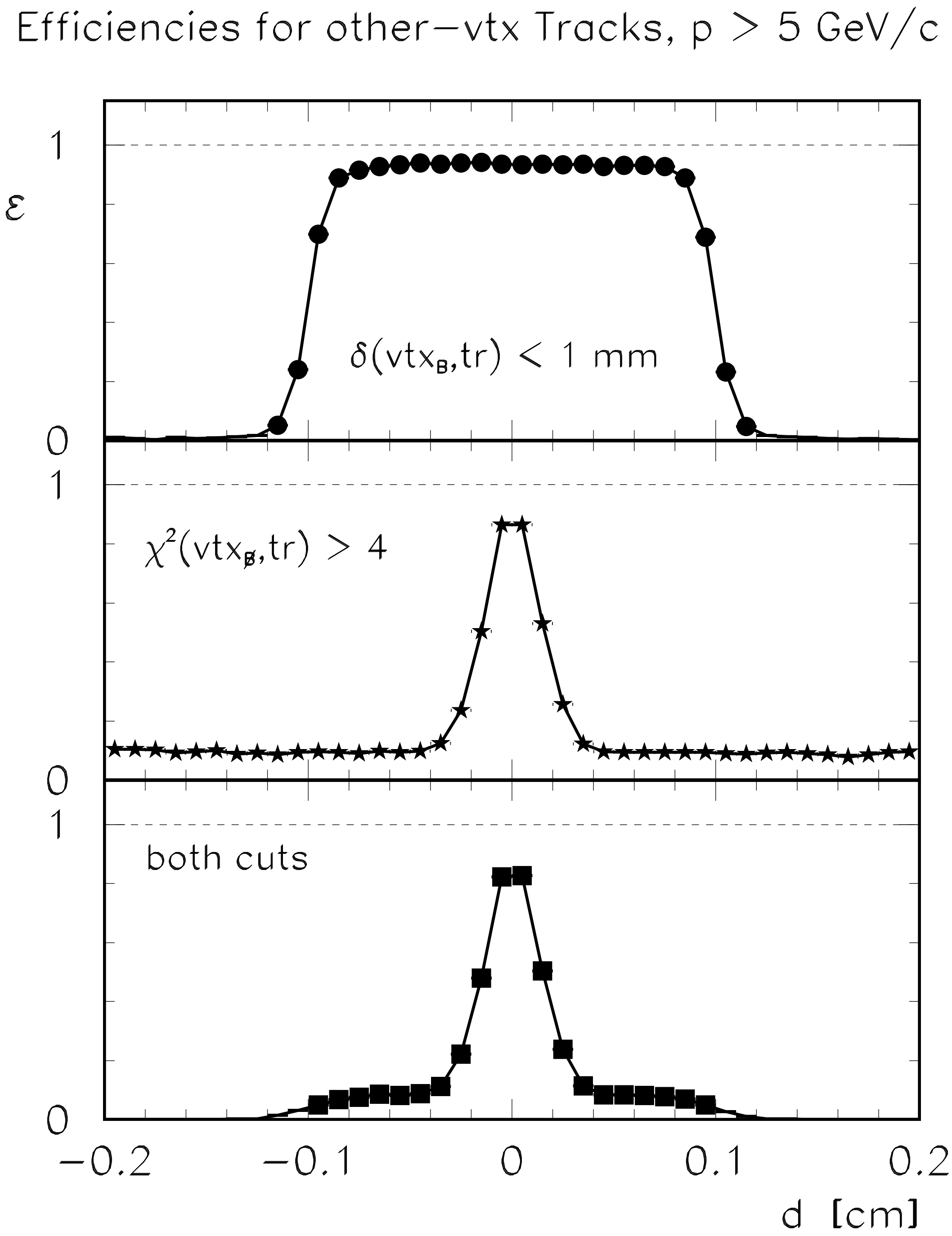

Figure 7: *Probabilities (as function of the distance d between the generated B vertex and MB vertex) for hard tracks from reconstructed MB vertices to survive typical cleaning cuts applied in the tagging algorithms.*

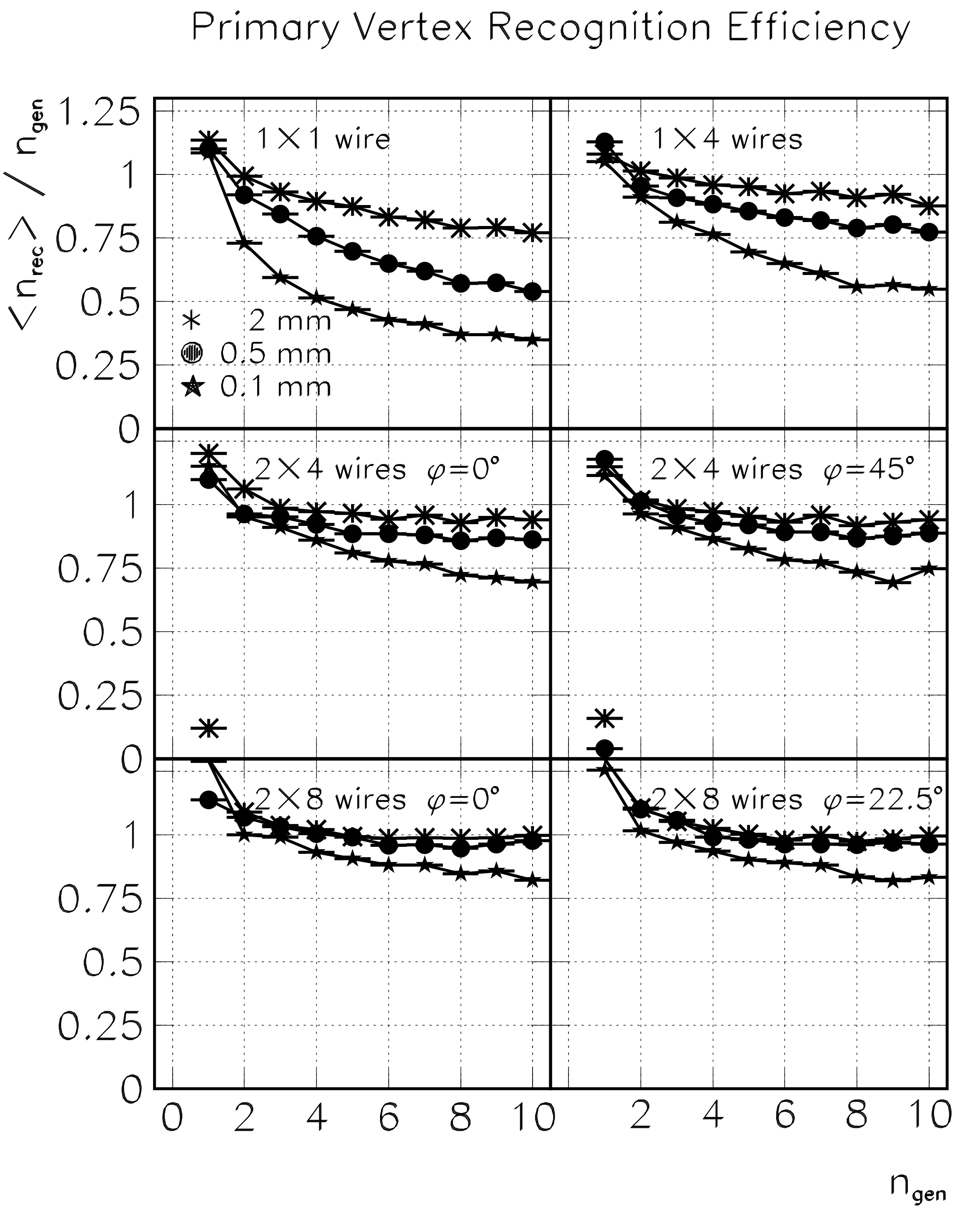

Figure 8: *Mean number of reconstructed vertices, n_{rec}, normalized to the number of generated vertices, n_{gen}, as function of n_{gen}, displayed for all target geometries considered and for three different values of the beam halo width. Note that the B vertex is by definition always reconstructed, so that n_{rec} is never smaller than 1.*

3.2 The Lepton Tag

Figs. 9–11 display, as functions of the halo width, the efficiencies of the various cuts of the tagging procedure for correct (wrong) sign leptons from the tagging B decay, and for fake leptons from other vertices. Correct (wrong) sign means that the sign of the charge of the tagging lepton is the same (the inverse) as that for the beauty quark in the tagging B hadron. A fake tag is a particle not stemming from the tagging B decay which is either a true lepton or a misidentified lepton. Similar definitions are used for the other tagging methods. The plots are shown separately for all six wire target configurations.

The following cuts are applied for identified leptons (or faked leptons):

1. Momentum cuts: The momentum is required to be larger than $5\,\mathrm{GeV}/c$, the transverse momentum to be larger than $0.8\,\mathrm{GeV}/c$. Fig. 9 shows that this cut is very effective, since it suppresses very strongly the background due to fake leptons and to a lesser extent the wrong sign signal. As expected, the momentum cuts have the same performance for all wire configurations and are independent of the halo width.

2. B vertex compatibility cut: The distance between the B vertex and the lepton candidate track is required to be less than $1\,\mathrm{mm}$. As can be seen from Fig. 10 this cut reduces the lepton tagging efficiency by about 25% but typically cuts down the fake leptons by more than a factor 2. Only in the case of a single-wire target, this cut becomes fully useless, since signal and background are reduced by comparable amounts. It is interesting to note that for the other configurations the cut stays operational for the full range of σ_{Halo} considered.

3. MB vertex veto cut: The χ^2 distance between any reconstructed MB vertex and the lepton candidate track is required to be larger than 4 (the number of degrees of freedom is 2 for this χ^2). Fig. 11 shows that this cut tends to be inefficient for the case of the lepton tag. It should be probably left out for optimal performance. Only for the case of a single-wire target the cut reduces the fake background significantly and therefore compensates some of the inefficiency of the previous cut. No drastic dependence of the cut performance on σ_{Halo} is observed.

3.3 The Kaon Tag

Figs. 12–15 display, as functions of the halo width, the efficiencies of the various cuts of the tagging procedure for correct (wrong) sign kaons from the tagging B decay, and for fake kaons from other vertices. The plots are shown separately for all six wire target configurations.

The following cuts are applied for identified kaons (or faked kaons):

1. Momentum cuts: The momentum is required to be larger than $5\,\mathrm{GeV}/c$ and smaller than $50\,\mathrm{GeV}/c$. Fig. 12 shows that this cut is effective, since it suppresses significantly the background due to fake tag candidates. Contrary to the lepton tag, the wrong sign signal (due to wrong sign kaons from the tagging B decay) is not suppressed. As expected, the momentum cuts have the same performance for all wire configurations and are independent of the halo width.

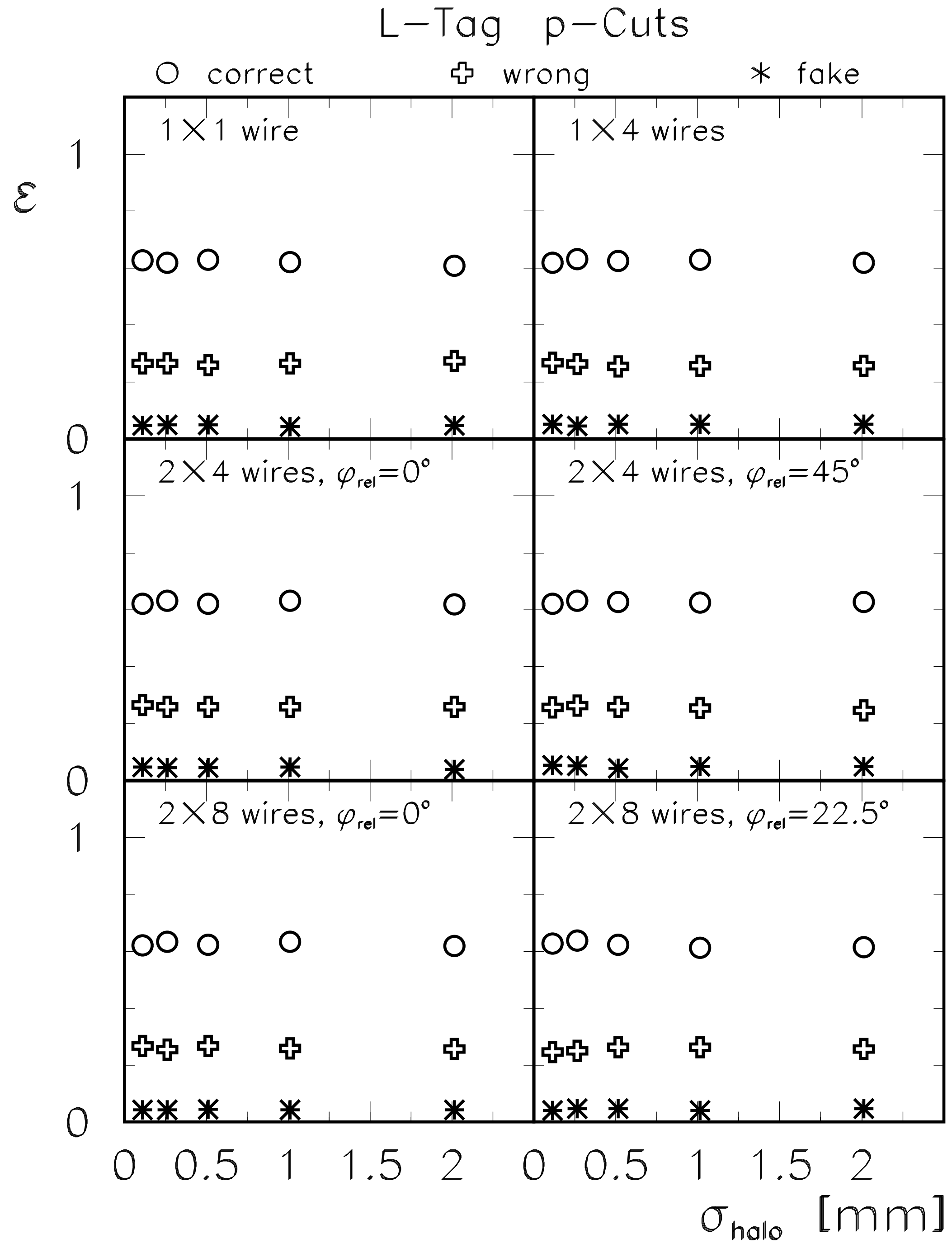

Figure 9: *Efficiency as function of the halo width of the momentum cuts applied to lepton tag candidates (separately for leptons from the tagging B decay with correct charge or wrong charge, and for fake candidates not originating from the tagging B decay). All wire configurations considered are shown separately.*

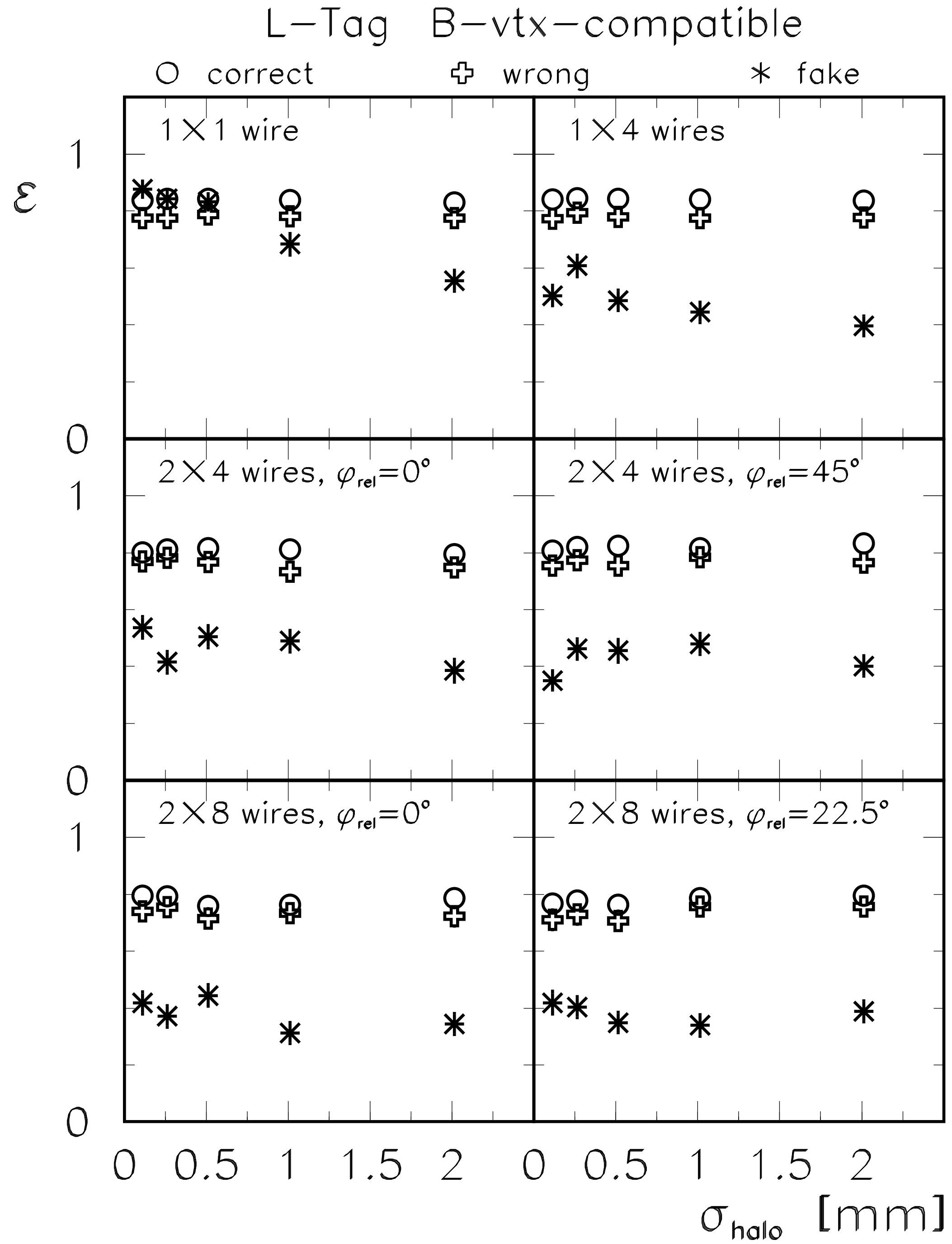

Figure 10: *Efficiency as function of the halo width of the B vertex compatibility cut applied to lepton tag candidates (separately for leptons from the tagging B decay with correct charge or wrong charge, and for fake candidates not originating from the tagging B decay). All wire configurations considered are shown separately.*

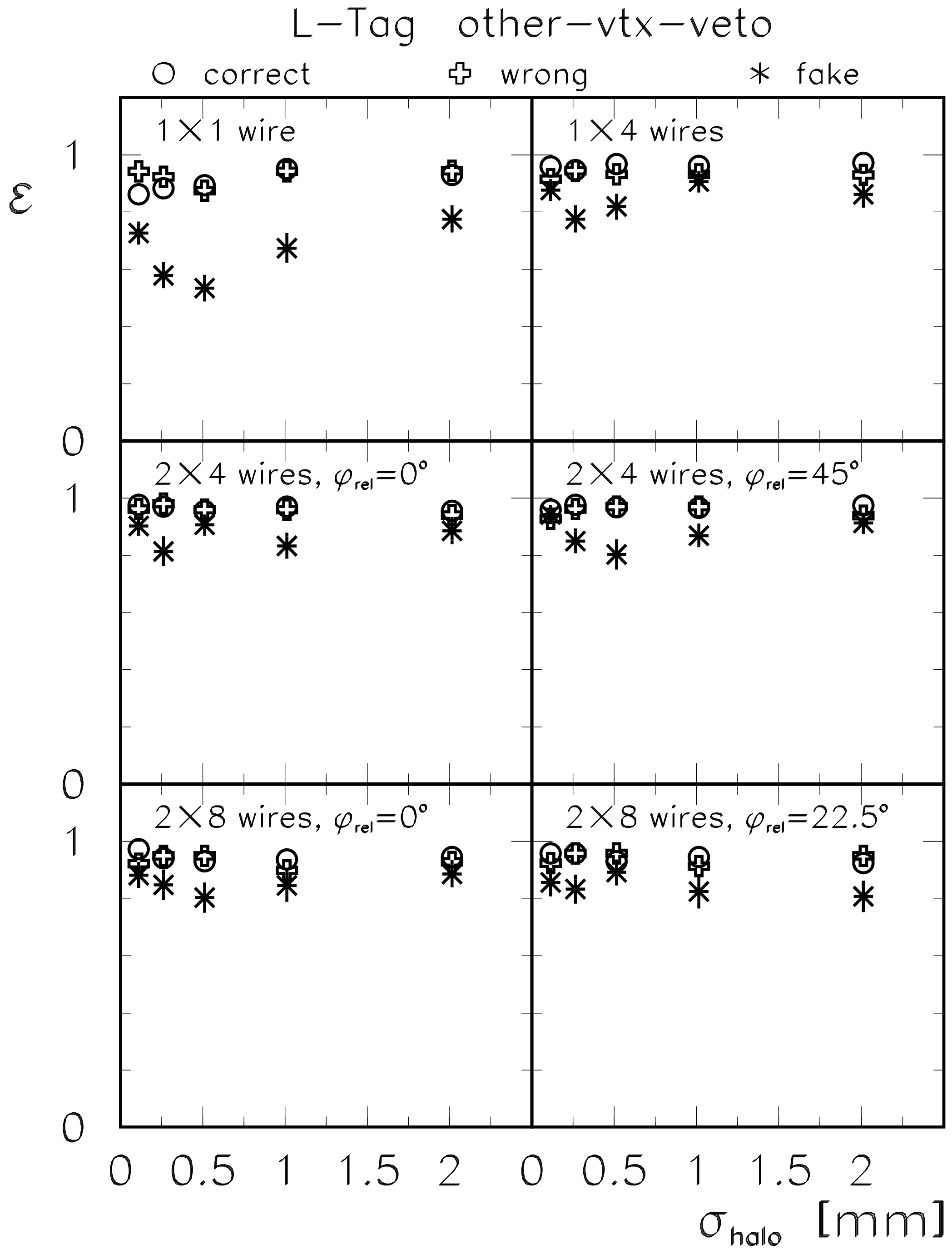

Figure 11: *Efficiency as function of the halo width of the non-B vertex veto cut applied to lepton tag candidates (separately for leptons from the tagging B decay with correct charge or wrong charge, and for fake candidates not originating from the tagging B decay). All wire configurations considered are shown separately.*

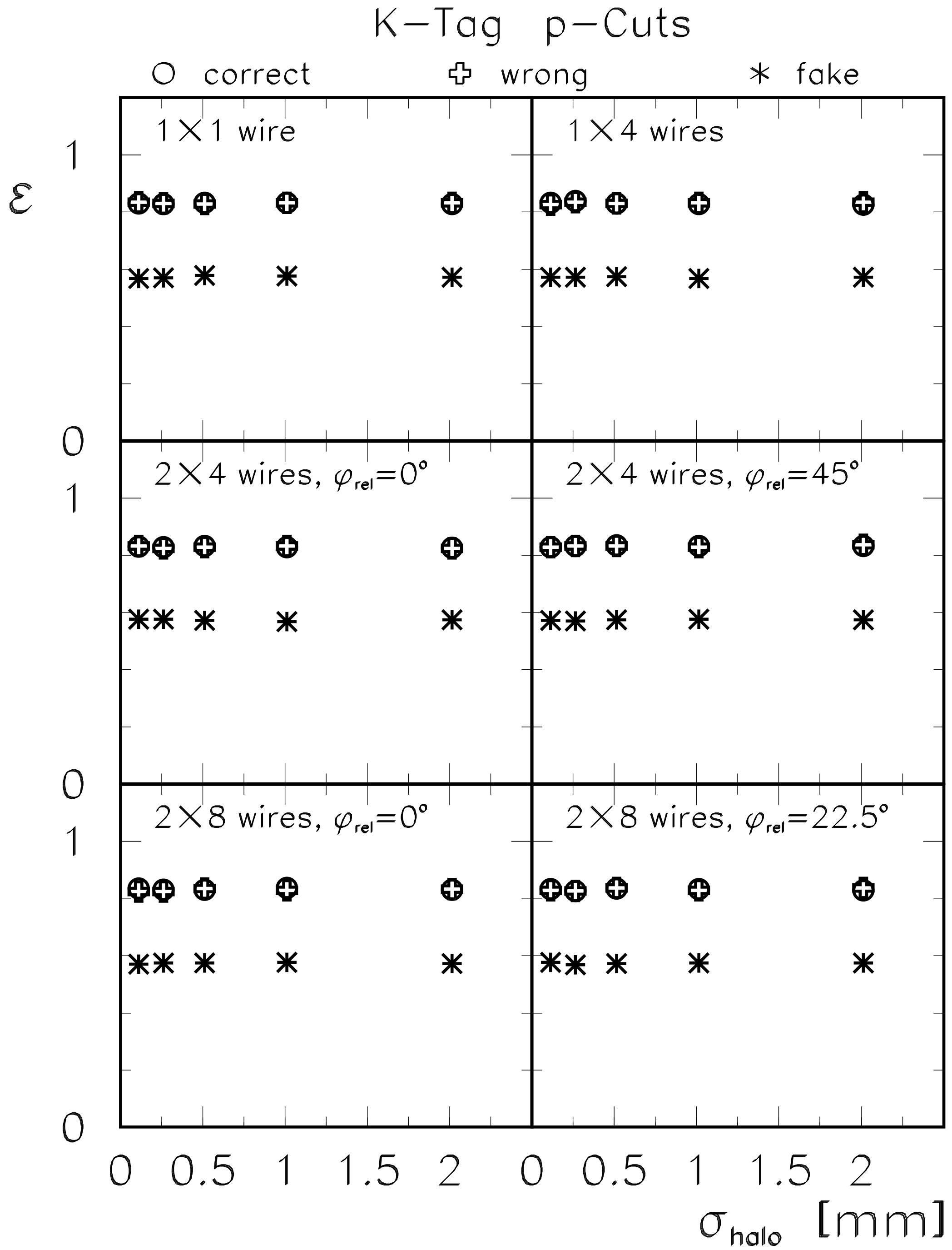

Figure 12: *Efficiency as function of the halo width of the momentum cuts applied to kaon tag candidates (separately for kaons from the tagging B decay with correct charge or wrong charge, and for fake candidates not originating from the tagging B decay). All wire configurations considered are shown separately.*

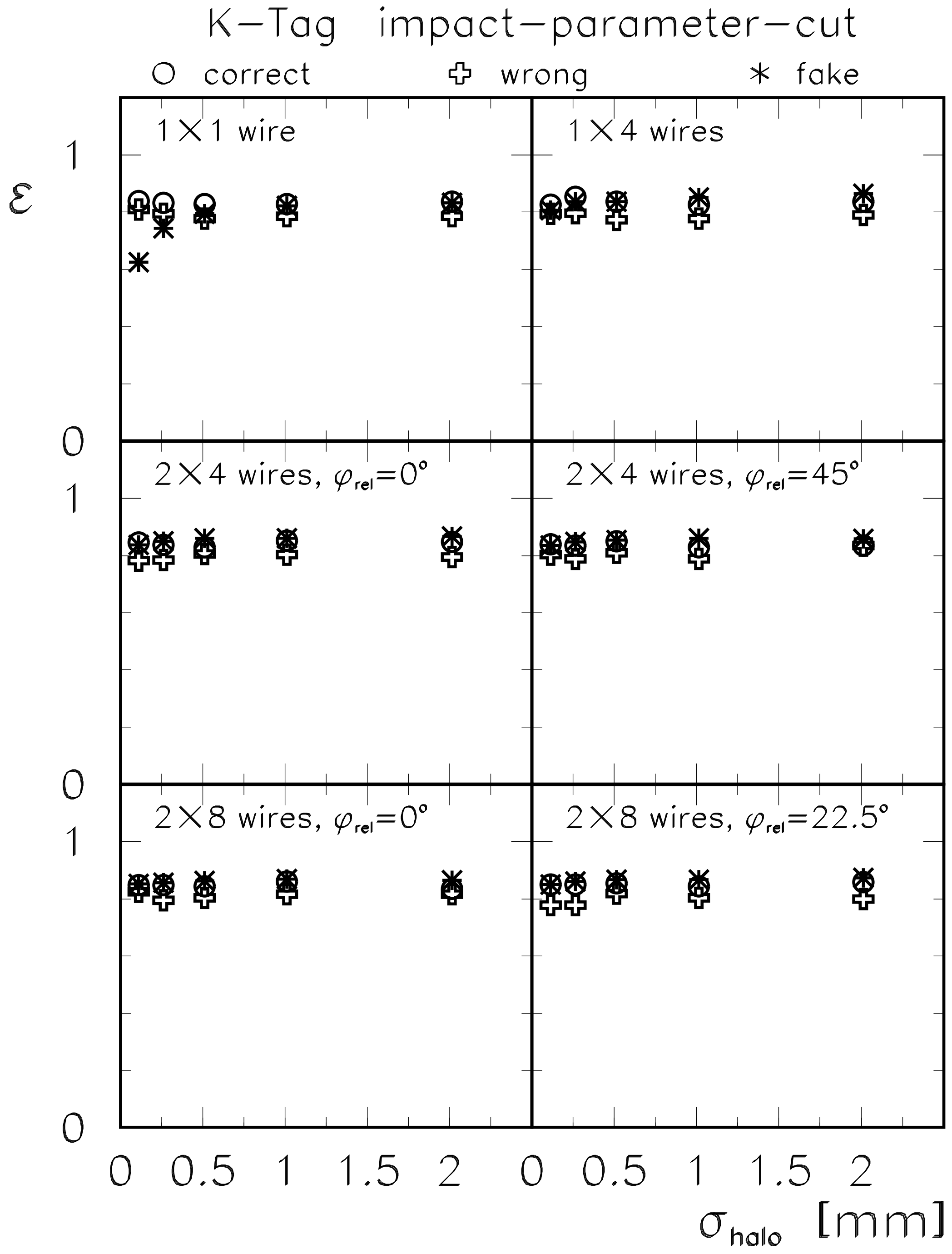

Figure 13: *Efficiency as function of the halo width of the impact parameter cut applied to kaon tag candidates (separately for kaons from the tagging B decay with correct charge or wrong charge, and for fake candidates not originating from the tagging B decay). All wire configurations considered are shown separately.*

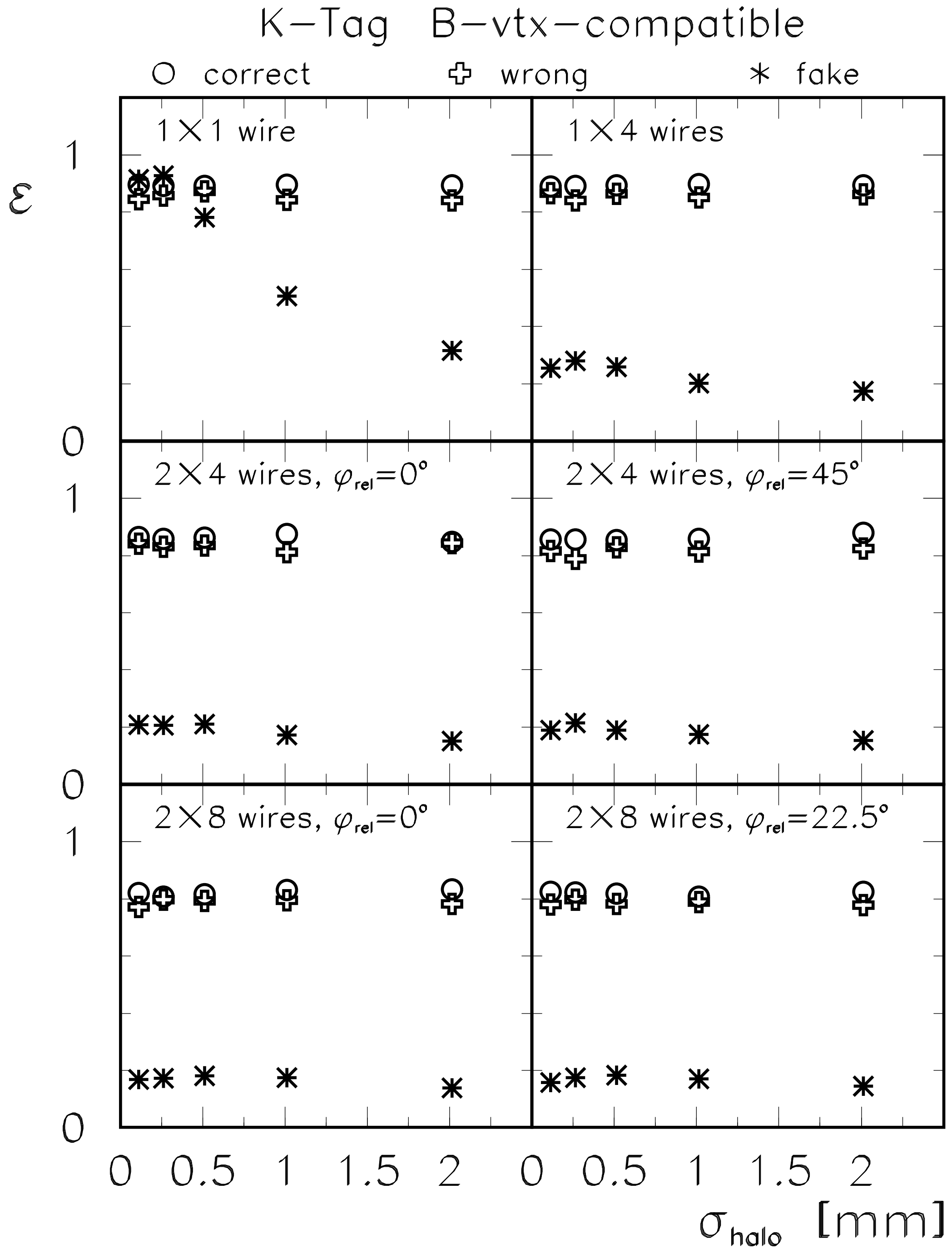

Figure 14: *Efficiency as function of the halo width of the B vertex compatibility cut applied to kaon tag candidates (separately for kaons from the tagging B decay with correct charge or wrong charge, and for fake candidates not originating from the tagging B decay). All wire configurations considered are shown separately.*

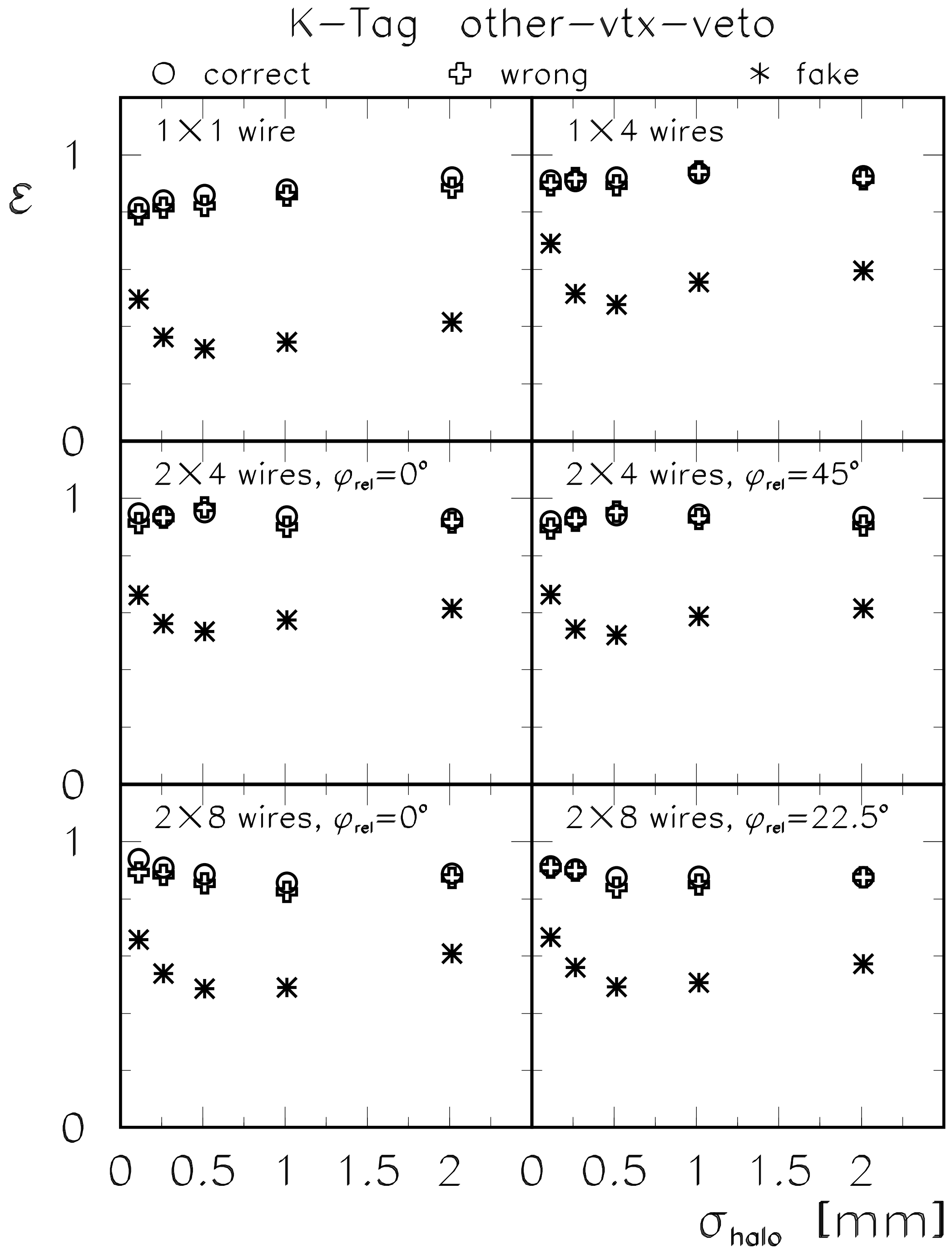

Figure 15: *Efficiency as function of the halo width of the non-B vertex veto cut applied to kaon tag candidates (separately for kaons from the tagging B decay with correct charge or wrong charge, and for fake candidates not originating from the tagging B decay). All wire configurations considered are shown separately.*

2. Impact parameter cut: The χ^2 distance between the B vertex and the tag candidate track is required to be larger than 2. As can be seen from Fig. 13, this cut depends very little on the wire configuration and on the halo width. Also, the cut is quite useless (if not harmful) since it reduces signal and background by the same amount. It should probably be left out for optimal performance.

3. B vertex compatibility cut: The distance between the B vertex and the kaon tag candidate track is required to be less than 1 mm. As can be seen from Fig. 14 this cut reduces the kaon tagging efficiency by about 20% but typically cuts down the fake tags by a factor 4. Only in the case of a single-wire target, this cut becomes useless for $\sigma_{Halo} < 1\,\mathrm{mm}$. It is interesting to note that for the other configurations the cut stays operational for the full range of σ_{Halo} considered.

4. MB vertex veto cut: The χ^2 distance between any reconstructed MB vertex and the kaon tag candidate track is required to be larger than 4 (the number of degrees of freedom is 2 for this χ^2). Fig. 15 shows that, contrary to the case of the lepton tag, this cut is very efficient, reducing the fake background by almost a factor 2 while keeping most of the kaon candidates from the tagging B decays. A degradation of the performance is observed towards very small values of the halo width, $\sigma_{Halo} < 250\,\mu\mathrm{m}$. For the case of a single-wire target the cut performs somewhat better than for the multi-wire targets, thus compensating some of the inefficiency of the previous cut.

3.4 The Charge Tag

The charge tag is based on all tracks which survive the cuts. They are used to compute an average linearly momentum-weighted charge. The sign of this quantity is finally used for the tagging decision. Figs. 16–18 display, as functions of the halo width, the efficiencies of the various cuts of the tagging procedure for correct (wrong) sign tracks from the tagging B decay, and for fake tag candidates from other vertices. All plots are independently shown for all six wire targets.

The following cuts are applied for all charged tracks:

1. Assignment to secondary vertex or impact parameter cut: Tracks which are assigned to a secondary vertex in the secondary vertex pattern recognition (which has extremely poor performance) are accepted. In addition, all charged tracks with a χ^2 distance from the B vertex exceeding 2 are kept. As can be seen from Fig. 16, this cut depends very little on the wire configuration and on the halo width. Only for the single-wire target at smallest values for σ_{Halo} the reduction of fake candidates becomes slightly more effective. The cut is in total not very efficient but might not be useless, since the charge tag is computed from a momentum weighted sum. No attempt was made to understand the details of this cut in more depth.

2. B vertex compatibility cut: The distance between the B vertex and the charge tag candidate track is required to be less than 1 mm. As can be seen from Fig. 17 this cut reduces the charge tagging track multiplicity by about 30% but typically cuts down the fake track multiplicity by more than a factor 4. Only in the case of a single-wire

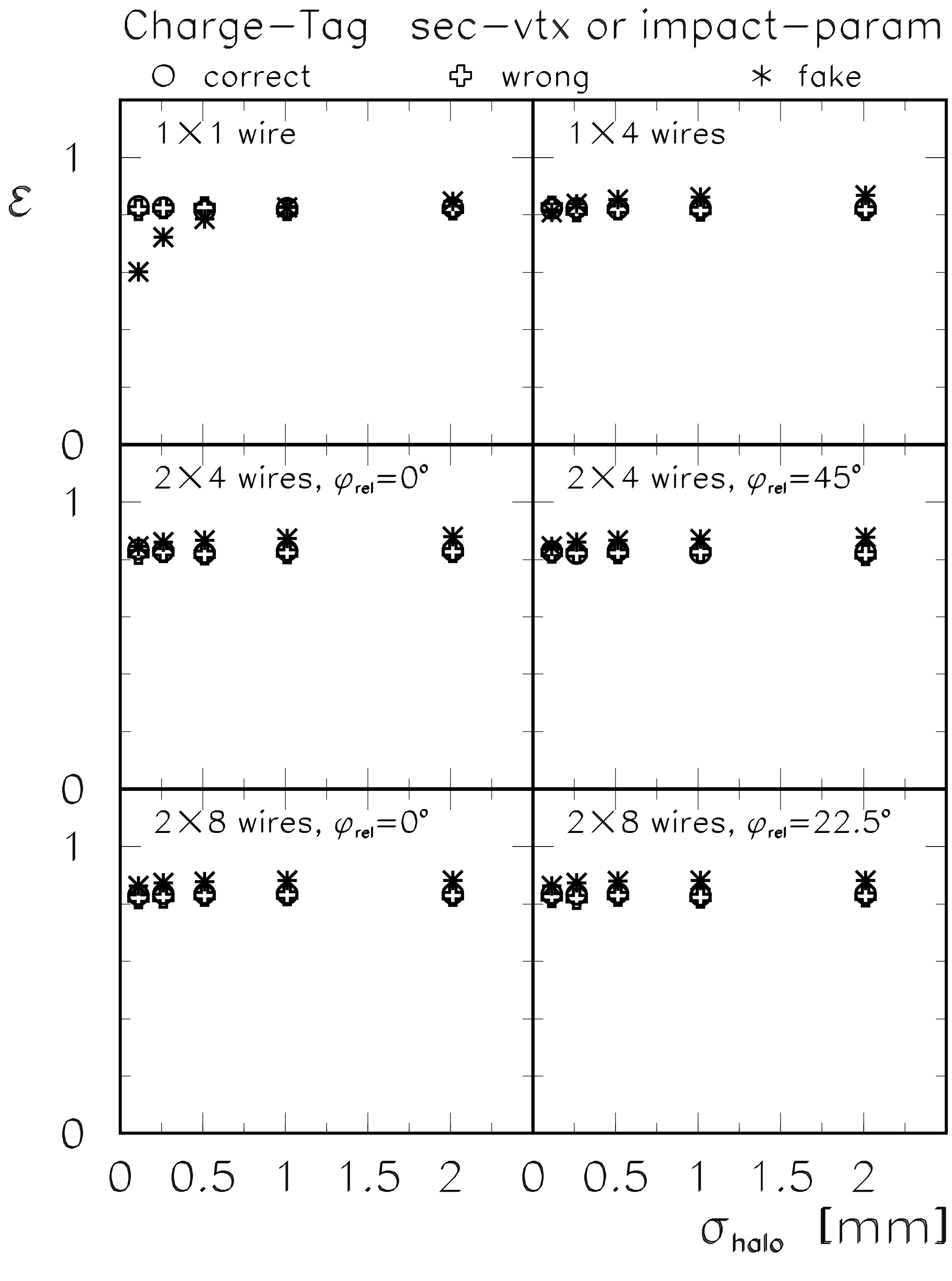

Figure 16: *Combined efficiency as function of the halo width of the secondary vertex assignment or impact parameter cut applied to charge tag track candidates (separately for tracks from the tagging B decay with correct charge or wrong charge, and for fake candidates not originating from the tagging B decay). All wire configurations considered are shown separately.*

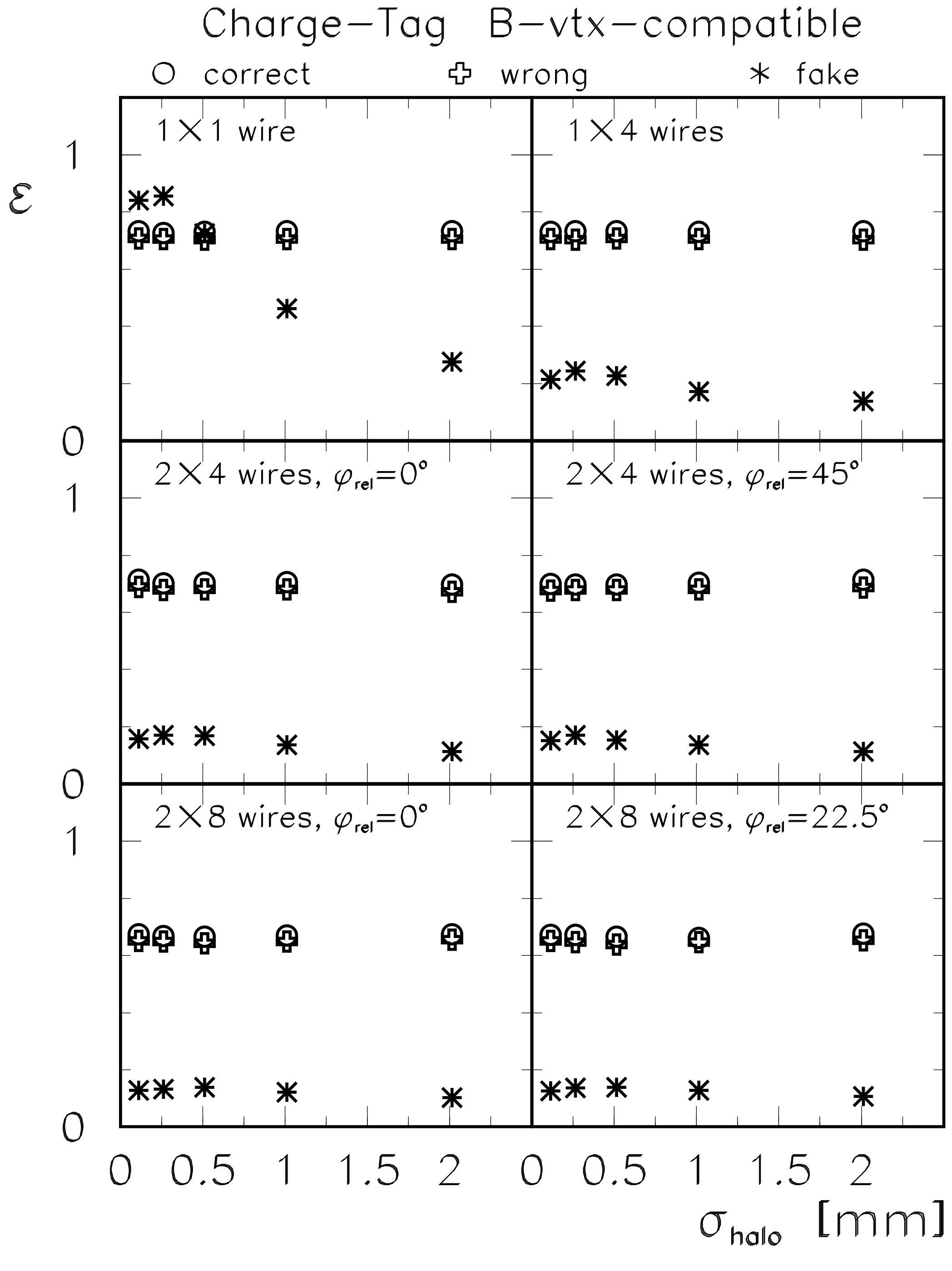

Figure 17: *Efficiency as function of the halo width of the B vertex compatibility cut applied to charge tag track candidates (separately for tracks from the tagging B decay with correct charge or wrong charge, and for fake candidates not originating from the tagging B decay). All wire configurations considered are shown separately.*

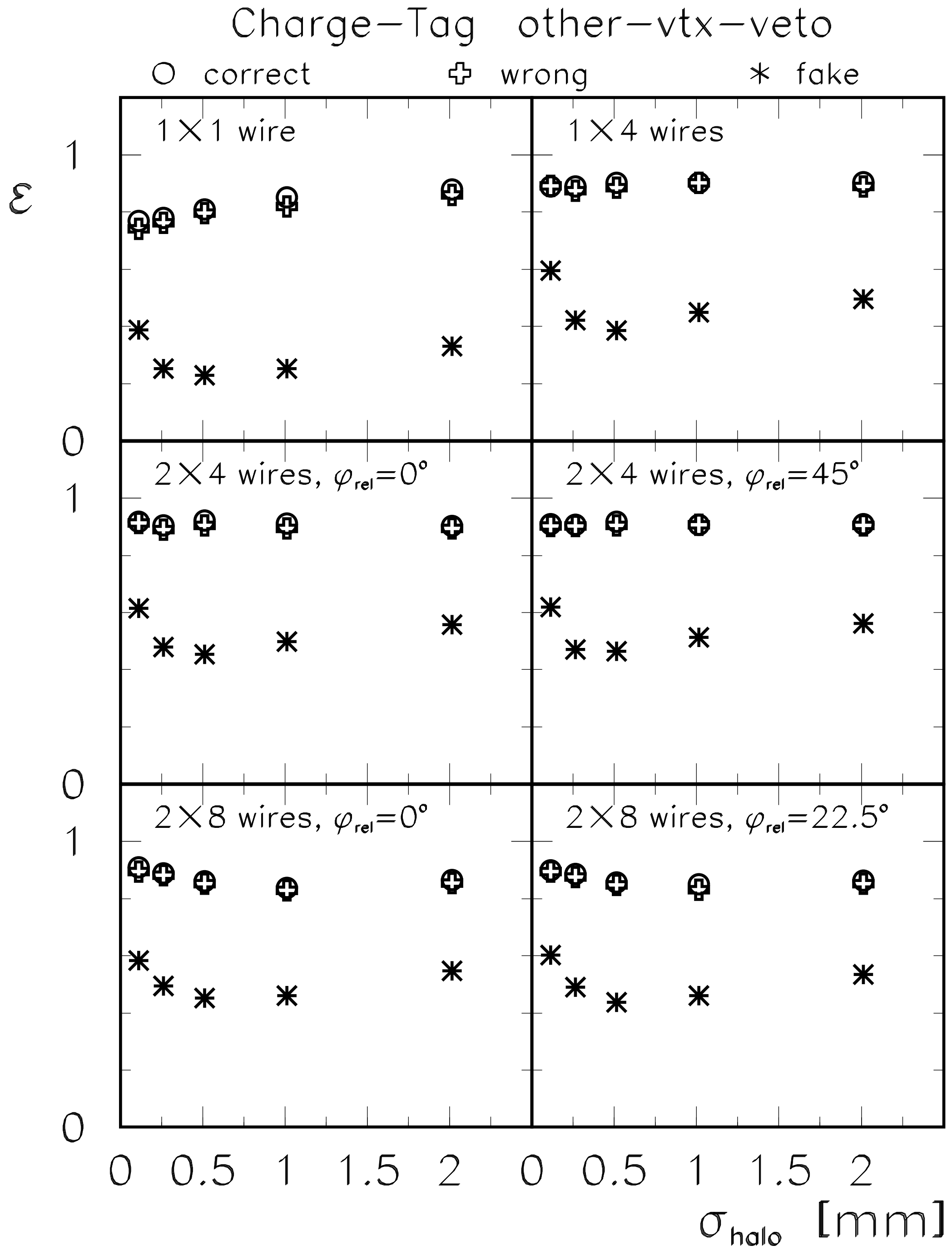

Figure 18: *Efficiency as function of the halo width of the non-B vertex veto cut applied to charge tag track candidates (separately for tracks from the tagging B decay with correct charge or wrong charge, and for fake candidates not originating from the tagging B decay). All wire configurations considered are shown separately.*

target, this cut becomes useless for $\sigma_{Halo} < 1\,\mathrm{mm}$. It is interesting to note that for the other configurations the cut stays operational for the full range of σ_{Halo} considered.

3. MB vertex veto cut: The χ^2 distance between any reconstructed MB vertex and the charge tag candidate track is required to be larger than 5 (the number of degrees of freedom is 2 for this χ^2). Fig. 18 shows that, contrary to the case of the lepton tag and similarly to the case of the kaon tag, this cut is very efficient, reducing the fake track multiplicity by typically a factor 2 while keeping most of the track candidates from the tagging B decays. A degradation of the performance is observed towards very small values of the halo width, $\sigma_{Halo} < 250\,\mu\mathrm{m}$. For the case of a single-wire target the cut performs somewhat better than for the multi-wire targets, thus compensating some of the inefficiency of the previous cut.

3.5 Study of Tagging Performances

The quality of the tagging performance, resulting from the cuts described in the previous subsections, can be best characterized by the tagging efficiency, the dilution factor, and the statistical power of a tag. If N_B is the number of observed B decays into a channel sensitive to CP violation, only the fraction $\epsilon \cdot N_B$ of these events will be accompanied by a tag, if ϵ is the efficiency for finding a tag. The error of the CP violation measurement is hence increased by a factor $1/\sqrt{\epsilon}$, compared to ideal tagging. If amongst the $\epsilon \cdot N_B$ tags there are N_c correct-sign and N_w wrong-sign tags, then the CP signal is in addition diluted, increasing the error again by a factor $1/D$, where

$$D = \frac{N_c - N_w}{N_c + N_w} \tag{2}$$

is the dilution factor. In total, the error increases by a factor $1/\kappa$, where

$$\kappa = D \cdot \sqrt{\epsilon} \tag{3}$$

is the statistical power of the tag.

The results of the systematic studies for lepton tag, kaon tag, and charge tag are summarized in Figs. 19–21 which display the tagging efficiencies, dilution factors, and statistical powers for all three tags and all six target configurations as functions of the halo width. The results are surprisingly unspectacular. In some cases, especially for targets consisting of a small number of wires, the dilution factor decreases towards smaller halo width, but this effect is always partly compensated by an simultaneously rising tagging efficiency. The tagging power, which is the only quantity relevant for the final performance of the experiment, shows almost no dependence on the halo width or the wire configuration. Only for unrealistically small values of σ_{Halo} some mild deterioration of kaon and charge tag is observed. In addition, the single wire target performs slightly worse than the multi-wire configurations.

3.6 Analysis of Multi-Tag Situations

The overall precision of the CP violation measurements uses all available tags (probably more kinds than considered here). This means that the tagging methods have to be combined. The

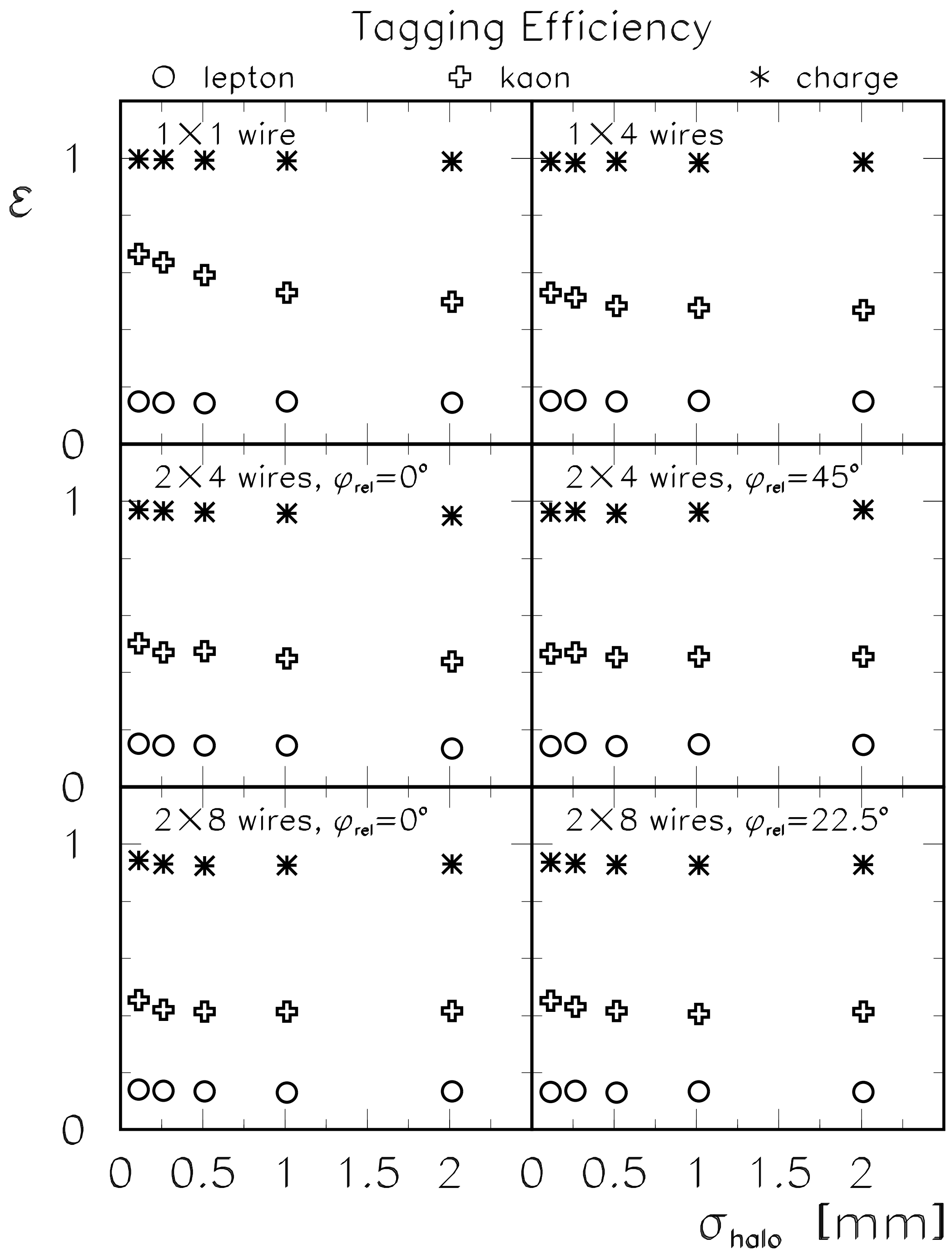

Figure 19: *Tagging efficiency as function of the halo width for lepton, kaon and charge tag. All wire configurations considered are shown separately.*

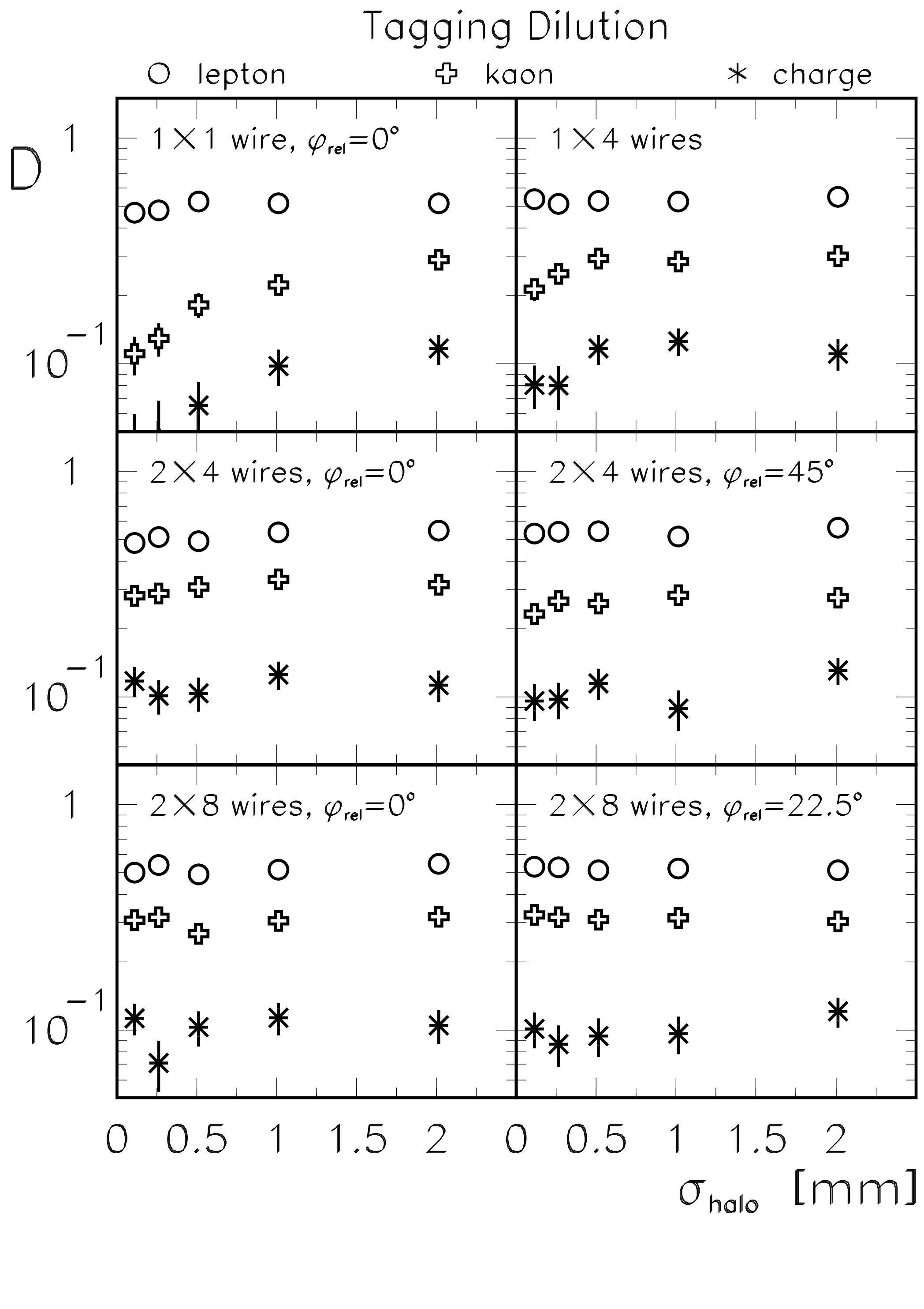

Figure 20: *Tagging dilution as function of the halo width for lepton, kaon and charge tag. All wire configurations considered are shown separately.*

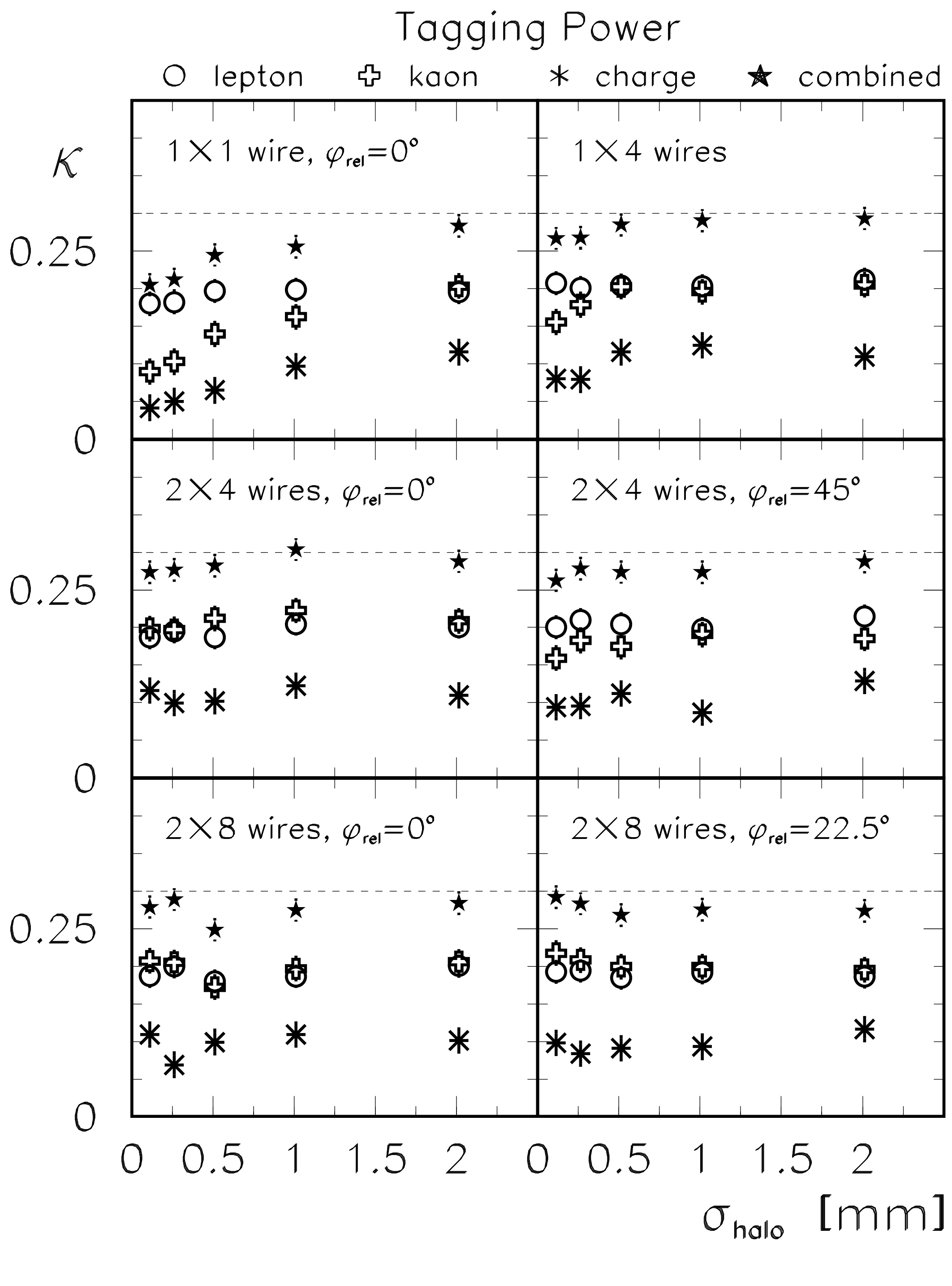

Figure 21: *Statistical tagging power as function of the halo width for lepton, kaon and charge tag, and for the combination of all three tags. All wire configurations considered are shown separately.*

procedure has been decribed in the proposal: One splits the data sample into independent classes, where each class has a certain combination of positive and negative tags active. For illustration, all possible classes of three-tag (lepton, kaon, charge) situations, two-tag situations (one tag not active due to missing detectors) and single-tag situations are listed in table 2 (single group of four wires) and in table 3 (two groups of four wires, not rotated) for $\sigma_{Halo} = 500\,\mu$m. In the overall tagging sign of a certain class, the highest priority is given to the lepton tag. If this is not present, the kaon tag defines the overall tagging sign. If the kaon tag is also missing, the charge tag is used. A missing tag is denoted by "0". The highest priority active tag is denoted by "+". Any other tag is denoted by "+" ("−") if it agrees (disagrees) with the highest priority tag. The tables list the number of B decays, N_B, reconstructed from the Monte Carlo data sample, the number of correct (N_c) and wrong (N_w) sign tags, the total number of tags, N_{tag}, and the efficiency, dilution factor, and statistical power for each class.

As explained in detail in the appendix (section 5), it is very simple to combine these independent classes. The tagging power can, for example, be computed from the quadratic sum of the tagging powers of the independent tagging classes. The result for the combined power of lepton, kaon, and charge tags is displayed in Fig. 21 together with the individual tags. As can be seen, for realistic halo widths, all wire configurations reach tagging powers close to 0.3, with exception of a single-wire target which reaches values around 0.25. The single-group or double-group four-wire targets perform quite optimally. No advantage of higher wire multiplicity or rotated wire groups is apparent.

4 Conclusions

This note investigated the performance of tagging procedures for the CP violation measurement in the decay $B^0 \to J/\psi K^0_S$. A large variety of target wire configurations and assumptions on the width of the halo have been tested. The investigations show that

- the B production vertex is of very high quality and is stable against merging with minimum bias vertices down to distances of $200\,\mu$m along the target wire.
- primary vertex recognition is very robust up to highest vertex multiplicities.
- the tagging performance does not deteriorate down to $\sigma_{Halo} \approx 500\,\mu$m, as long as the target is not reduced below a number of four wires.
- no advantage of more than four wires per target group can be observed.
- no advantage of rotating the two wire groups azimuthally with respect to each other can be observed.

In conclusion, as far as the CP violation measurement in the golden channel is concerned, there is no necessity to modify the present target mechanics. Also, it might be advisable to operate the target with a single group of four wires and leave the second group as spare.

These conclusions could of course be inadequate for the performance of the target for other physics topics (other CP channels, B_s mixing etc.) or for the performance of special trigger types on the second trigger level. Further studies might be necessary in this direction.

L	K	Q	N_B	N_{tag}	N_c	N_w	ϵ	D	κ
0	**0**	+	3191	1359	699	660	0.4259	0.0287	0.0187
0	+	−	3191	422	260	162	0.1322	0.2322	0.0845
0	+	**0**	3191	0	0	0	0.0000	0.0000	0.0000
0	+	+	3191	900	588	312	0.2820	0.3067	0.1629
+	−	−	3191	36	18	18	0.0039	0.0000	0.0000
+	−	**0**	3191	0	0	0	0.0000	0.0000	0.0000
+	−	+	3191	50	32	18	0.0157	0.2800	0.0350
+	**0**	−	3191	68	53	15	0.0213	0.5588	0.0816
+	**0**	**0**	3191	2	2	0	0.0006	1.0000	0.0250
+	**0**	+	3191	189	149	40	0.0592	0.5767	0.1404
+	+	−	3191	20	16	4	0.0063	0.6000	0.0475
+	+	**0**	3191	0	0	0	0.0000	0.0000	0.0000
+	+	+	3191	114	96	18	0.0357	0.6842	0.1293
total			3191	3160			**0.9903**	**0.2864**	**0.2850**

	K	Q	N_B	N_{tag}	N_c	N_w	ϵ	D	κ
	0	+	3191	1616	863	753	0.5064	0.0681	0.0484
	+	−	3191	492	294	198	0.1542	0.1951	0.0766
	+	**0**	3191	0	0	0	0.0000	0.0000	0.0000
	+	+	3191	1050	702	348	0.3291	0.3371	0.1934
total			3191	3158			**0.9897**	**2147**	**0.2136**

L		Q	N_B	N_{tag}	N_c	N_w	ϵ	D	κ
0		+	3191	2681	1449	1232	0.8402	0.0809	0.0742
+		−	3191	124	87	37	0.0389	0.4032	0.0795
+		**0**	3191	2	2	0	0.0006	1.0000	0.0250
+		+	3191	353	277	76	0.1106	0.5694	0.1894
total			3191	3160			**0.9903**	**0.2209**	**0.2198**

L	K		N_B	N_{tag}	N_c	N_w	ϵ	D	κ
0	+		3191	1322	848	474	0.4143	0.2829	0.1821
+	−		3191	86	50	36	0.0270	0.1628	0.0267
+	**0**		3191	259	204	55	0.0812	0.5753	0.1639
+	+		3191	134	112	22	0.0420	0.6716	0.1376
total			3191	1801			**0.5644**	**0.3758**	**0.2823**

L			N_B	N_{tag}	N_c	N_w	ϵ	D	κ
+			3191	479	366	113	**0.1501**	**0.5282**	**0.2046**

	K		N_B	N_{tag}	N_c	N_w	ϵ	D	κ
	+		3191	1542	996	546	**0.4832**	**0.2918**	**0.2029**

		Q	N_B	N_{tag}	N_c	N_w	ϵ	D	κ
		+	3191	3158	1763	1395	**0.9897**	**0.1165**	**0.1159**

Table 2: *Combination of tagging efficiencies (ϵ), dilutions (D), statistical powers (κ) for all three-tag, two-tag and single-tag scenarios for configuration 8 in table 1 (single group of 4 wires, halo width 500μm).*

L	K	Q	N_B	N_{tag}	N_c	N_w	ϵ	D	κ
0	**0**	+	3195	1307	672	635	0.4091	0.0283	0.0181
0	+	−	3195	422	271	151	0.1320	0.2844	0.1033
0	+	**0**	3195	1	1	0	0.0003	1.0000	0.0177
0	+	+	3195	886	583	303	0.2773	0.3160	0.1664
+	−	−	3195	36	16	20	0.0113	−0.1111	−0.0118
+	−	**0**	3195	0	0	0	0.0000	0.0000	0.0000
+	−	+	3195	50	33	17	0.0156	0.3200	0.0400
+	**0**	−	3195	71	57	14	0.0222	0.6056	0.0903
+	**0**	**0**	3195	4	3	1	0.0013	0.5000	0.0177
+	**0**	+	3195	179	136	43	0.0560	0.5196	0.1230
+	+	−	3195	19	16	3	0.0059	0.6842	0.0528
+	+	**0**	3195	0	0	0	0.0000	0.0000	0.0000
+	+	+	3195	105	85	20	0.0329	0.6190	0.1122
total			3195	3080			**0.9640**	**0.2876**	**0.2824**
	K	Q	N_B	N_{tag}	N_c	N_w	ϵ	D	κ
	0	+	3195	1557	822	735	0.4873	0.0559	0.0390
	+	−	3195	491	304	187	0.1537	0.2383	0.0934
	+	**0**	3195	1	1	0	0.0003	1.0000	0.0177
	+	+	3195	1027	688	339	0.3214	0.3398	0.1927
total			3195	3076			**0.9628**	**0.2226**	**0.2184**
L		Q	N_B	N_{tag}	N_c	N_w	ϵ	D	κ
0		+	3195	2615	1406	1209	0.8185	0.0753	0.0682
+		−	3195	126	89	37	0.0394	0.4127	0.0820
+		**0**	3195	4	3	1	0.0013	0.5000	0.0177
+		+	3195	334	254	80	0.1045	0.5210	0.1694
total			3195	3079			**0.9637**	**0.2038**	**0.2001**
L	K		N_B	N_{tag}	N_c	N_w	ϵ	D	κ
0	+		3195	1309	855	454	0.4097	0.3063	0.1961
+	−		3195	86	49	37	0.0269	0.1395	0.0229
+	**0**		3195	254	196	58	0.0795	0.5433	0.1532
+	+		3195	124	101	23	0.0388	0.6290	0.1239
total			3195	1773			**0.5549**	**0.3744**	**0.2789**
L			N_B	N_{tag}	N_c	N_w	ϵ	D	κ
+			3195	464	346	118	**0.1452**	**0.4914**	**0.1873**
	K		N_B	N_{tag}	N_c	N_w	ϵ	D	κ
	+		3195	1519	993	526	**0.4754**	**0.3074**	**0.2120**
		Q	N_B	N_{tag}	N_c	N_w	ϵ	D	κ
		+	3195	3075	1697	1378	**0.9624**	**0.1037**	**0.1018**

Table 3: *Combination of tagging efficiencies (ϵ), dilutions (D), statistical powers (κ) for all three-tag, two-tag and single-tag scenarios for configuration 13 in table 1 (two groups of 4 wires, no relative rotation, halo width 500 μm).*

5 Appendix: How to Combine Several Tags

If one observes N_B B decays in the channel used for a CP violation measurement, the error on the CP asymmetry is given by

$$\sigma_{CP} = \frac{\sigma_0}{\sqrt{N_B}} \tag{4}$$

in the case of ideal flavour tagging, where $1/\sigma_0$ is the statistical power per observed B decay. In a realistic measurement, this error is increased due to non-perfect flavour tagging. Let N_c (N_w) be the number of correct (wrong) sign tags of a certain class (e.g. lepton or kaon tag). Then the error is increased

1. by the inverse of a dilution factor

$$D = \frac{N_c - N_w}{N_c + N_w} \quad , \tag{5}$$

2. due to the reduction of useful B decays by the tagging efficiency

$$\epsilon = \frac{N_c + N_w}{N_B} \quad . \tag{6}$$

Therefore, the final error of the CP measurement reads

$$\sigma_{CP} = \frac{1}{\kappa} \cdot \frac{\sigma_0}{\sqrt{N_B}} \quad , \tag{7}$$

where

$$\kappa = D \cdot \sqrt{\epsilon} \tag{8}$$

is the statistical power of the tag.

The quantities ϵ, D, κ can be extracted from Monte Carlo simulations. For N_B generated B decays the statistical precisions of these estimates are

$$\sigma_\epsilon = \frac{1}{\sqrt{N_B}} \cdot \sqrt{\epsilon(1-\epsilon)} \tag{9}$$

$$\sigma_D = \frac{1}{\sqrt{N_B}} \cdot \sqrt{\frac{1-D^2}{\epsilon}} \tag{10}$$

$$\sigma_\kappa = \frac{1}{\sqrt{N_B}} \cdot \sqrt{1 - \frac{3+\epsilon}{4} \cdot D^2} \quad . \tag{11}$$

If n disjoint classes of tags are available, each characterized by efficiency ϵ_i, dilution factor D_i, and statistical power κ_i, with $i = 1 \ldots n$, then n independent CP violation measurements can be performed, with corresponding precisions

$$\sigma_{CP}^{(i)} = \frac{1}{\kappa_i} \cdot \frac{\sigma_0}{\sqrt{N_B}} \quad . \tag{12}$$

The weighted average of these measurements has the combined precision

$$\sigma_{CP} = \left[\sum_{i=1}^{n} \frac{1}{\sigma_{CP}^{(i)\ 2}}\right]^{-1/2} = \frac{1}{\left[\sum_{i=1}^{n} \kappa_i^2\right]^{1/2}} \cdot \frac{\sigma_0}{\sqrt{N_B}} \quad . \tag{13}$$

This argument shows that the tagging powers of the independent classes must be added in quadrature. Since in addition the combined tagging efficiency is of course just the linear sum of the individual efficiencies, one finally arrives at the following combined tagging quality parameters:

$$\kappa = \sqrt{\sum_{i=1}^{n} \kappa_i^2} \tag{14}$$

$$\epsilon = \sum_{i=1}^{n} \epsilon_i \tag{15}$$

$$D = \frac{\kappa}{\sqrt{\epsilon}} = \sqrt{\sum_{i=1}^{n} \frac{\epsilon_i}{\epsilon} \cdot D_i^2} \quad . \tag{16}$$

The statistical precision of these quantities, if obtained from a Monte Carlo simulation with N_B simulated B decays, can be conveniently computed by the following expressions:

$$\sigma_\kappa = \frac{1}{\sqrt{N_B}} \cdot \sqrt{1 - \frac{1}{4}\kappa^2 - \frac{3}{4}\sum_{i=1}^{n} \left(\frac{\kappa_i}{\kappa}\right)^2 D_i^2} \tag{17}$$

$$\sigma_\epsilon = \frac{1}{\sqrt{N_B}} \cdot \sqrt{\epsilon\,(1-\epsilon)} \tag{18}$$

$$\sigma_D = \frac{1}{\sqrt{N_B}} \cdot \frac{1}{\sqrt{\epsilon}} \cdot \sqrt{1 - \frac{1}{4}D^2 - \frac{3}{4}\sum_{i=1}^{n} \left(\frac{\kappa_i}{\kappa}\right)^2 D_i^2} \quad . \tag{19}$$